*Journal of Paleontology*

**www.cambridge.org/jpa**

# Constraining the Ediacaran–Cambrian boundary in South China using acanthomorphic acritarchs and uniserial modular microfossils

Orin M. Lole Durbin[1], Kenneth H. O'Donnell[2] and Shuhai Xiao[1]

[1]Department of Geosciences, Virginia Tech, Blacksburg, VA 24061, USA
[2]Geosyntec Consultants Inc., 1900 L Street NW, Washington, DC 20036, USA

## Articles

**Cite this article:** Lole Durbin O.M., O'Donnell K.H., and Xiao S. 2026. Constraining the Ediacaran–Cambrian boundary in South China using acanthomorphic acritarchs and uniserial modular microfossils. *Journal of Paleontology*, **100**(3), 499–518
https://doi.org/10.1017/jpa.2026.10247

Received: 02 December 2025 UTC
Revised: 01 April 2026 UTC
Accepted: 22 April 2026 UTC

**Corresponding author:**
Shuhai Xiao;
Email: xiao@vt.edu

**Handling Editor:**
Joseph Botting

## Abstract

The Ediacaran–Cambrian boundary, representing one of Earth's most critical transitions, is currently defined by the Fortune Head (Newfoundland, Canada) GSSP (Global Standard Stratotype Section and Point) at a point once regarded as the first appearance of the branching trace fossil *Treptichnus pedum*. However, *T. pedum* has subsequently been found below the GSSP, and its global distribution is primarily restricted to siliciclastic facies where application of alternative biostratigraphic and chemostratigraphic correlation tools is challenging. Investigations of acanthomorphic acritarchs in basal Cambrian strata of South China suggest that these microfossils could provide a robust complementary biostratigraphic marker for the Ediacaran–Cambrian boundary. Acanthomorphic acritarchs are widely distributed across the Yangtze Platform in chert–phosphorite layers intercalated with carbonates and shales, thereby allowing their biostratigraphic occurrences to be calibrated with small shelly fossil biozones and carbon isotope data.

Here, the earliest Cambrian *Asteridium–Heliosphaeridium–Comasphaeridium* (AHC) assemblage biozone is identified at 11 localities within the Yanjiahe, lower Niutitang, and upper Liuchapo formations, representing diverse depositional environments. Two latest Ediacaran microfossils, both characterized by uniserially chained modules and representing a characteristic Ediacaran assemblage (the *Horodyskia minor–Nenoxites jiumenensis*, or HmNj, assemblage biozone), are also identified in the Liuchapo Formation, but do not overlap with the Cambrian AHC acritarch biozone. The AHC assemblage biozone is demonstrated to be stratigraphically equivalent to basal Cambrian small shelly fossils and a negative $\delta^{13}C$ isotope excursion known to occur at the Ediacaran–Cambrian boundary. Thus, in South China, the AHC and HmNj assemblage biozones can be used to effectively and reliably constrain the Ediacaran–Cambrian boundary.

UUID: http://zoobank.org/2fd52705-f7ef-4276-897e-10e89efb04ad

## Non-technical Summary

The boundary between the Ediacaran (635–539 million years ago, Ma) and Cambrian (539–487 Ma) periods represents a critical transition in Earth history, with the dawn of the Phanerozoic (539–0 Ma) bringing a rapid increase in the diversity and complexity of life. Currently, this important boundary is defined by the first appearance of complex burrowing behaviors exhibited by early marine organisms, recorded in the rock record as trace fossils. However, because the appearance of these trace fossils is restricted to particular rock types, they are difficult to correlate with supplemental boundary indicators, such as skeletal remains of early animals and diagnostic chemical excursions.

Investigating earliest Cambrian deposits in South China has revealed that spiny organic-walled microfossils, or acritarchs, can serve as a useful marker for the Ediacaran–Cambrian boundary. These acritarchs are widely distributed in a variety of rock types preserved across South China, allowing their occurrences to be reliably correlated with other boundary indicators. These acritarchs are also demonstrated to be equivalent in time to other markers, indicating their suitability for recognizing the boundary. Acritarchs were identified at 11 localities across a shallow- to deep-water transect on the Yangtze Craton in South China, signifying their broad environmental distribution. Consequently, these acritarchs are determined to be a robust boundary marker in South China. Additionally, two latest Ediacaran microfossils, consisting of strings of bead-like and crescentic modules, are shown to be characteristic of late Ediacaran rocks, providing an additional constraint on the Ediacaran–Cambrian boundary. This study demonstrates that, in South China, acritarchs and modular microfossils can be used to effectively and reliably bracket the Ediacaran–Cambrian boundary.

© The Author(s), 2026. Published by Cambridge University Press on behalf of Paleontological Society. This is an Open Access article, distributed under the terms of the Creative Commons Attribution-NonCommercial-NoDerivatives licence (http://creativecommons.org/licenses/by-nc-nd/4.0), which permits non-commercial re-use, distribution, and reproduction in any medium, provided that no alterations are made and the original article is properly cited. The written permission of Cambridge University Press or the rights holder(s) must be obtained prior to any commercial use and/or adaptation of the article.

JOURNAL OF PALEONTOLOGY
A PUBLICATION OF THE Paleontological SOCIETY

CAMBRIDGE UNIVERSITY PRESS

## Introduction

The Ediacaran–Cambrian transition represents a critical evolutionary event in Earth history, with an observed rapid diversification of biomineralizing, burrowing, planktonic, and nektonic organisms in the rock record (Alroy, 2010; Wood and Zhuravlev, 2012; Nowak et al., 2015; Mángano and Buatois, 2017) accompanied by abrupt, drastic changes in ocean chemistry (Maloof et al., 2010). Effectively defining and recognizing the Ediacaran–Cambrian boundary in sedimentary successions is essential for characterizing the tempo and mode of environmental and ecological changes during this crucial transition.

The first appearance of the complex trace fossil *Treptichnus pedum* (Seilacher, 1955) Jensen, 1997, at Fortune Head (Newfoundland, Canada) was selected as the Global Standard Stratotype Section and Point (GSSP) for the Ediacaran–Cambrian boundary (Narbonne et al., 1987; Landing, 1994). In subsequent work, the first appearance of *T. pedum* was observed several meters below the original GSSP (Gehling et al., 2001). *Treptichnus pedum* is an ichnofossil exhibiting multiple branching probes, hypothesized to represent burrows of early priapulid animals (Vannier et al., 2010), identified worldwide (Buatois, 2018), and shown to tolerate a broad range of environmental conditions in siliciclastic facies (Buatois et al., 2013). The appearance of this ichnofossil signifies the earliest known widespread complex burrowing and undermat mining behaviors (Herringshaw et al., 2017), which made it the preferred choice for defining the Ediacaran–Cambrian boundary (Narbonne et al., 1987; Landing, 1994).

Recently, *T. pedum* has come under scrutiny as a suitable biostratigraphic marker (Landing et al., 2013; Babcock et al., 2014; Buatois, 2018). The challenge of using the first occurrence of *T. pedum* to define the Ediacaran–Cambrian boundary is principally a result of its facies dependence; that is, *T. pedum* primarily occurs within siliciclastics. This complicates correlation between siliciclastic successions and those dominated by carbonates, which frequently lack trace fossils but contain other biostratigraphic markers, such as small shelly fossils (SSFs) or chemostratigraphic data in the form of $\delta^{13}C$ isotope profiles (Topper et al., 2022), prompting reconsiderations of the official definition of the Ediacaran–Cambrian boundary (e.g., Babcock et al., 2014).

Microfossils represent a possible additional biostratigraphic constraint on the Ediacaran–Cambrian boundary. A notable increase in the abundance and diversity of acanthomorphic acritarchs is observed at the base of the Cambrian (Knoll, 1994; Huntley et al., 2006; Moczydłowska, 2011). Among these acritarchs, the *Asteridium–Heliosphaeridium–Comasphaeridium* (AHC) assemblage zone (Yao et al., 2005) is particularly important for recognizing the base of the Cambrian System in South China. The AHC assemblage comprises a group of acanthomorphic acritarchs—*Asteridium tornatum* (Volkova, 1968) Moczydłowska, 1991, *Heliosphaeridium ampliatum* (Wang, 1985) Yao et al., 2005, and *Comasphaeridium annulare* (Wang, 1985) Yao et al., 2005—that co-occur with tubular microfossils, such as *Megathrix longus* Yin, 1987a, and various SSFs.

Regional correlation of the AHC biozone has been employed across South and Northwest China (Yao et al., 2005; Dong et al., 2009; Ahn and Zhu, 2017; Luo and Zhu, 2025), while global correlations have been made to acritarch assemblages of the Eastern European Platform (Moczydłowska, 1991; Yao et al., 2005), India (Tiwari, 1999), and possibly Kazakhstan (Sergeev and Ogurtsova, 1989). Additionally, uppermost Ediacaran strata in South China contain the characteristic microfossils *Horodyskia minor* Dong et al., 2008, and *Nenoxites jiumenensis* (Dong et al., 2008) n. comb., both consisting of uniserial modules (Dong et al., 2008; Chen and Feng, 2019; Zhu et al., 2019). The possibility of using Cambrian and Ediacaran microfossil assemblages to identify the Ediacaran–Cambrian boundary has, thus far, received little attention.

Here, we propose using Cambrian acanthomorphic acritarchs in conjunction with the Ediacaran microfossils *H. minor* and *N. jiumenensis* to bracket the Ediacaran–Cambrian boundary, providing a consistent and reliable biostratigraphic constraint, in South China. To test the validity of this biostratigraphic regime, the stratigraphic occurrences of Ediacaran uniserial modular microfossils and early Cambrian acanthomorphic acritarchs are correlated across 14 localities on the Yangtze Craton of South China. We evaluated the consistency of key fossil occurrences across facies and depositional environments along a carbonate shelf-to-basin transition, assessed the potential of using the AHC and HmNj assemblage biozones to bracket the boundary in South China, and explored the possibility of utilizing this boundary proxy globally.

## Geological setting

Ediacaran–Cambrian deposition on the passive continental margin of the Yangtze Craton (Fig. 1) is represented by shelf facies in the northwest (which was further differentiated into the inner shelf, intrashelf lagoon, and shelf margin; Fig. 1.2) and slope and basinal facies toward the southeast (Figs. 1.2, 2). In the inner shelf and intrashelf lagoon facies, Ediacaran sediments are composed of mixed shales and dolostones of the Doushantuo (635–551 Ma) and Dengying (551–539 Ma) formations (Condon et al., 2005; Linnemann et al., 2019). These Ediacaran strata are disconformably overlain by Cambrian Yanjiahe Formation carbonates and shales, which underly younger Shuijingtuo Formation black shales (Figs. 1.3, 2). In shelf margin environments, a carbonate shoal developed during the Ediacaran Period, with intraclastic carbonates and interbedded shales deposited in northeastern Guizhou, northern Hunan, and southwestern Hubei provinces. Deepwater slope and basinal strata developed in the southeast of the Yangtze Block (Fig. 1.2). These deposits comprise Doushantuo Formation basinal black shales overlain by silicified mudstones and shales of the Ediacaran–Cambrian Liuchapo Formation, and then basinal black shales of the early Cambrian Niutitang Formation (Figs. 1.3, 2).

*Shelf facies.* On the shelf, Ediacaran–Cambrian boundary strata are represented by the carbonate-dominated Dengying Formation and the overlying Yanjiahe Formation (Fig. 2; Zhang et al., 2022). Characterized by interbedded shelf carbonates, gray to black shale, and cm-scale, black, organic-rich chert layers, the Yanjiahe Formation is interpreted to have been deposited during a marine transgression in a carbonate ramp setting (Jiang et al., 2011). The shelf is composed almost entirely of limestone and dolostone, with a gradual increase in phosphatic chert and shale content both vertically and towards the shelf edge.

The Yanjiahe Formation has been subdivided into five informal members based on lithostratigraphy (Guo et al., 2014). The lowermost member comprises interbedded silty dolostone and chert. Overlying this, the second member is defined by phosphatic, intraclastic, dolomitic wackestones and packstones containing the first SSF assemblage zone (i.e., the *Anabarites trisulcatus–Protohertzina anabarica* biozone [Guo et al., 2014]) and AHC microfossils (Dong et al., 2009; Ahn and Zhu, 2017), suggesting that the Ediacaran–Cambrian boundary is within this member (Yao et al., 2005; Guo et al., 2014; Steiner et al., 2020). This inference is further supported

https://doi.org/10.1017/jpa.2026.10247 Published online by Cambridge University Press

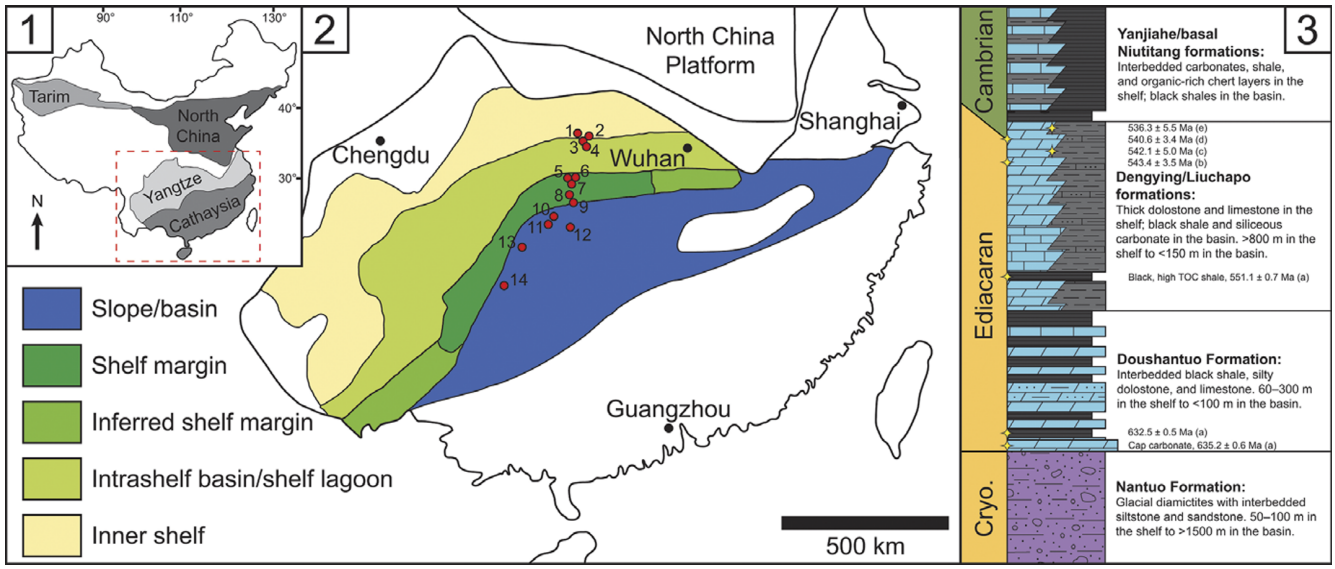



**Figure 1.** Geological context. (**1**) Location of the Yangtze Block, with dashed rectangle marking area enlarged in (**2**). (**2**) Generalized paleogeographic reconstruction for the Yangtze Platform during the terminal Ediacaran to early Cambrian, modified from Jiang et al. (2012). Studied localities include: Jiuqunao (1; 30°52'48.2"N, 110°52'54.0"E); Jijiapo (2; 30°45'10.8"N, 111°01'58.8"E); Baiguotang (3; 30°44'23.3"N, 110°58'04.0"E); Hezi'ao (4; 30°30'43.3"N, 111°09'03.4"E); Ganziping (5; 29°03'58.5"N, 110°26'43.8"E); Sancha (6; 29°03'57.6"N, 110°33'31.1"E); Daping (7; 29°00'47.1"N, 110°29'00.6"E); Siduping (8; 28°54'48.9"N, 110°27'02.1"E); Xugongping (9; 28°51'51.1"N, 110°27'54.5"E); Louyixi (10; 28°40'58.5"N, 109°58'45.4"E); Longbizui (11; 28°29'40.7"N, 109°50'35.4"E); Yanwutan (12; 28°24'48.7"N, 110°29'46.8"E); Taoying (13; 27°50'01.4"N, 109°01'04.9"E); and Jianxincun (14; 26°46'22.7"N, 108°25'01.0"E). (**3**) Generalized stratigraphy of the upper Cryogenian to lower Cambrian deposits on the Yangtze Platform. Stratigraphic age constraints (stars: left, shallow; right, deeper) are from: (a) Condon et al. (2005); (b) Huang et al. (2020); (c) Chen et al. (2015); (d) Zhang et al. (2022); (e) Chen et al. (2009).

by the presence of a pronounced negative $\delta^{13}C$ isotope excursion, inferred to be equivalent to the BAsal Cambrian Isotope Excursion (BACE), at stratigraphic levels coincident with or slightly below the AHC assemblage biozone (Ishikawa et al., 2008; Jiang et al., 2012; Ahn and Zhu, 2017). The third member consists of gray mudstone–wackestone interbedded with silty shale. A transition into carbonaceous limestones marks the fourth member. Finally, the fifth member is represented by gray intraclastic limestones preserving *Aldanella yanjiaheensis* Chen, 1984, and *Watsonella crosbyi* Grabau, 1900 (Guo et al., 2014, 2021), characteristic of the third SSF assemblage biozone (i.e., the *W. crosbyi* assemblage zone), which has been proposed to define the basal boundary of Cambrian Stage 2 (Peng et al., 2020; Steiner et al., 2020).

The Shuijingtuo Formation overlies the Yanjiahe Formation and represents a major marine transgression that deposited black shale facies above platform carbonates (Wang et al., 2012). The Shuijingtuo Formation can be divided into two informal members: a lower unit of black shale interbedded with nodular limestone, and an upper unit of silty shale and argillaceous limestone (Li and Holmer, 2004). In the lower Shuijingtuo Formation, an assemblage consisting of eodiscoid trilobites (Li et al., 2012), lingulid brachiopods (Li and Holmer, 2004; Broce et al., 2014), and bradoriids (Li et al., 2004) corresponds to Cambrian Stage 3 strata. A CA-ID-TIMS zircon U–Pb age of 526.43 ± 0.54 Ma from the basal Shuijingtuo Formation (Yang et al., 2023) provides a minimum age constraint on the underlying Yanjiahe Formation.

*Slope and basin facies.* In the slope and basin, Doushantuo Formation black shales underlie silicified shales of the Liuchapo Formation (Fig. 2); the silicified organic-rich Liuchapo shales are infrequently interbedded with silts and carbonates. The Liuchapo Formation is traditionally regarded as Ediacaran in age, coeval with the Dengying Formation (Zhu et al., 2003). However, a pronounced negative carbonate carbon isotope excursion of −10 ‰ is identified in the Liuchapo Formation (Chen and Feng, 2019), but not in the Dengying Formation (Ling et al., 2007; Ishikawa et al., 2008; Guo et al., 2013; Chen and Feng, 2019; Liu et al., 2025). A SIMS zircon U–Pb age of 540.7 ± 3.8 Ma reported from an ash bed two meters above this negative $\delta^{13}C_{carb}$ excursion indicates it can be correlated with the BACE (Chen and Feng, 2019), demonstrating that the Ediacaran–Cambrian boundary is preserved within the Liuchapo Formation. This assessment is also consistent with the numerous radiometric ages in the range of 546–535 Ma reported from the upper Liuchapo Formation (Fig. 1.3; e.g., Chen et al., 2015; Yang et al., 2017; Chen and Feng, 2019; Wang et al., 2020).

Overlying the Liuchapo Formation in slope-to-basin facies, the Niutitang Formation represents a major marine transgression with widespread deposition of black shale (Fig. 2). The Niutitang Formation can be subdivided into four informal units. The lowest unit is observed as a basal phosphoritic chert within the first meter of the formation. This unit is recognized in Hunan and Guizhou provinces and has been noted to contain sparse SSFs (Steiner et al., 2001; Zhang et al., 2001) and AHC taxa (Luo and Zhu, 2025). A laterally persistent, organic-rich, metalliferous, Ni-Mo-PGE sulfide ore layer, approximately 2 m above the base of the Niutitang, is utilized as a regional marker bed for correlation (Zhang et al., 2008; Wang et al., 2012). Niutitang strata above this ore layer comprise carbonaceous shales containing trilobites, bradoriids, and brachiopods (Peng and Babcock, 2001; Zhang et al., 2008), as well as articulated hexactinellid and demosponge fossils (Steiner et al., 1993; Luo and Reitner, 2019). Numerous studies have recovered ages of ca. 530–520 Ma for the basal Niutitang Formation (Jiang et al., 2009; Xu et al., 2011; Wang et al., 2012; Chen et al., 2015), indicating that the entirety of the formation is Cambrian in age, despite previous reports of ages at or around the Ediacaran–Cambrian boundary from presumed stratigraphic

https://doi.org/10.1017/jpa.2026.10247 Published online by Cambridge University Press

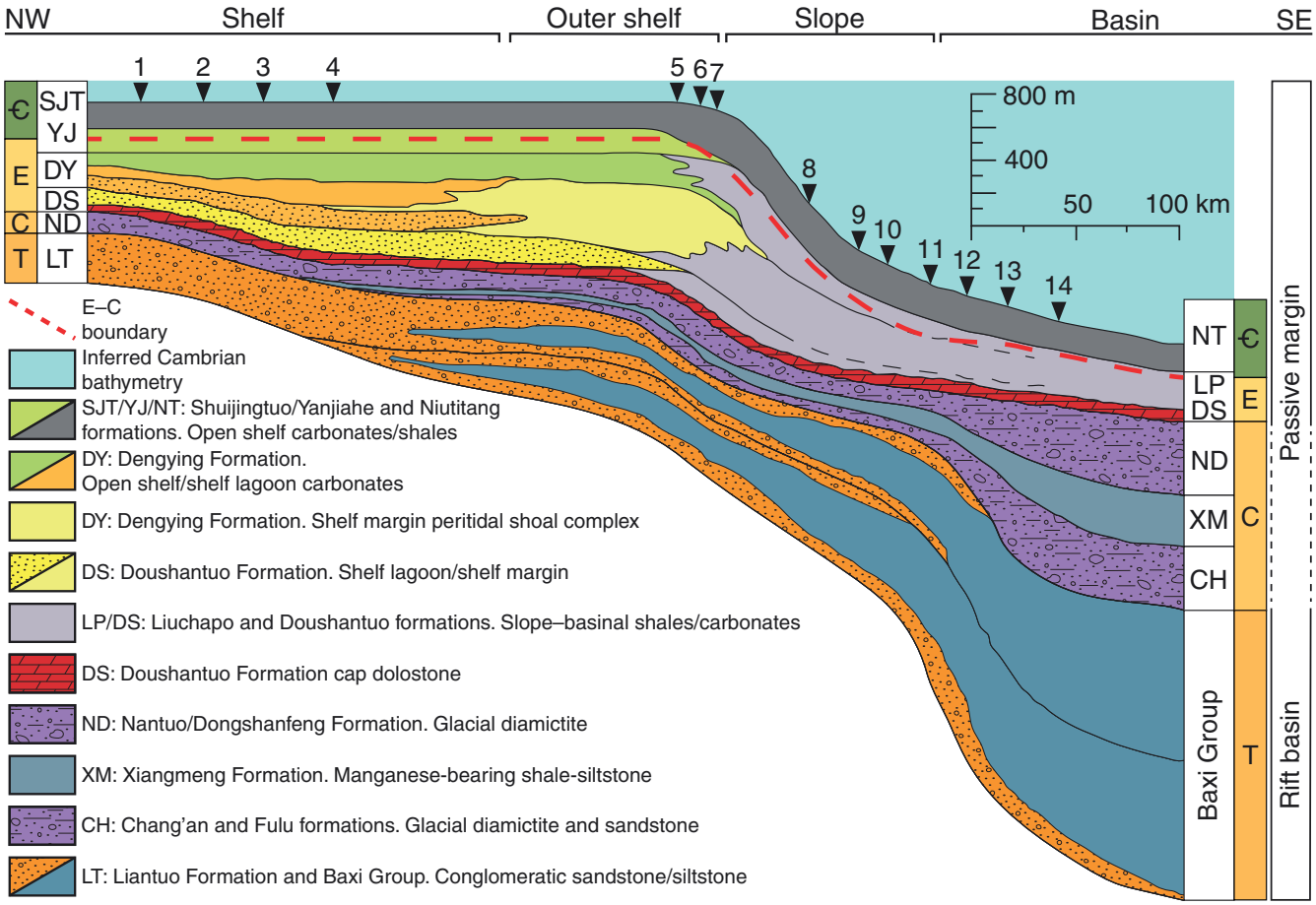



**Figure 2.** Schematic cross-section of the shelf-to-basin Tonian–Cambrian stratigraphy along a northwest–southeast transect of the Yangtze Platform. The Ediacaran–Cambrian boundary, as defined in this study, is illustrated by the red dashed line. C = Cryogenian; T = Tonian. Numbers correspond to localities in Figure 1, showing their approximate location along the transect. Modified from Jiang et al. (2011).

equivalents in shallow-water strata (Jenkins et al., 2002; Compston et al., 2008; Zhu et al., 2009).

## Materials and methods

Field sampling of strata undertaken in the summers of 2008 and 2011 focused on obtaining samples across the wide range of depositional environments represented by the uppermost Ediacaran and lowermost Cambrian Yangtze Craton shelf-to-basin transition successions in South China (Fig. 1.2). Sampling the Yanjiahe, Niutitang, and Liuchapo formations across several sections provided increased facies coverage, from shallow carbonate shelf to basinal black shale facies. Phosphatic chert of the Yanjiahe Formation, siliceous rocks of the Liuchapo Formation, and the basal Niutitang phosphorite bed were preferentially targeted to maximize fossil recovery; exquisitely preserved acritarchs are frequently associated with chert and phosphorite deposits (Yao et al., 2005; Dong et al., 2009; Guo et al., 2014).

Samples of nodular and bedded phosphatic cherts hosted in carbonates and silty mudstones, representing shelf facies, were collected from the Yanjiahe Formation at the Jiuqunao (1), Jijiapo (2), Baiguotang (3), and Hezi'ao (4) sections (Figs. 1.2, 2). Samples from the shelf margin, slope, and basin facies were collected from the Liuchapo and/or Niutitang formations at Ganziping (5), Sancha (6), Daping (7), Siduping (8), Xugongping (9), Louyixi (10), Longbizui (11), Yanwutan (12), Taoying (13), and Jianxincun (14) (Figs. 1.2, 2).

Samples ($n$ = 523) of phosphatic material, cherts, and siliceous sediments were collected, with stratigraphic heights/depths recorded from 14 measured sections along a 300 km north–south transect. Standard petrographic thin sections were prepared for all samples and examined on an Olympus BX51 petrographic microscope. Photographs were taken with an integrated Infinity1 digital camera. Abundances of observed microfossils were recorded on a per thin section basis.

*Repositories and institutional abbreviations.* Thin sections are reposited at the Virginia Polytechnic Institute Geosciences Museum (VPIGM), Blacksburg, Virginia, USA.

## Results

### *Lithostratigraphy*

Liuchapo Formation. The Liuchapo Formation (Fig. 3.1), which interdigitates with the Dengying Formation (Figs. 2, 3.2), consists of interbedded, silicified, black, organic-rich, and silty shales, in addition to thin, silicified, dolomitic mudstones (Fig. 3.3). The formation has a maximum thickness of only ~5–9 m on the shelf margin (Ganziping and Daping), but this increases basinward to 65 m at Longbizui. Phosphatic grains are uncommon in the basin (Louyixi,

https://doi.org/10.1017/jpa.2026.10247 Published online by Cambridge University Press

Longbizui, and Jianxincun) but increase in quantity moving towards the shelf (Daping, Siduping, and Xugongping).

The Liuchapo Formation can be divided into five distinct units. Unit 1, a peloidal-packed shale (0.2–10 m thick), forms the basal part of the Liuchapo Formation (Fig. 3.3). Peloids are generally no larger than 200 μm. This unit is observed at the base of the Liuchapo Formation between Daping, on the outermost shelf rim, and Jianxincun, in the deep basin. Disarticulated sponge spicules, preserved within micritic lithoclasts, are present at Ganziping. Planar bedded to laminated organic-rich black shales (0.2–7 m thick) represent Unit 2 and can be observed at Siduping, Louyixi, and Jianxincun. Unit 3 (0.5–3 m thick), present at Ganziping, Siduping, and Xugongping, is typified by convoluted laminae and massively layered shales with lithoclasts and disarticulated microfossils. Unit 4 comprises 0.2–2 m of dolomitic mudstones and silty shales, which occur near, or at the top of, the Liuchapo Formation in the outer shelf. This unit could be regarded as a facies continuation of the Dengying Formation given the interdigitate relationship between

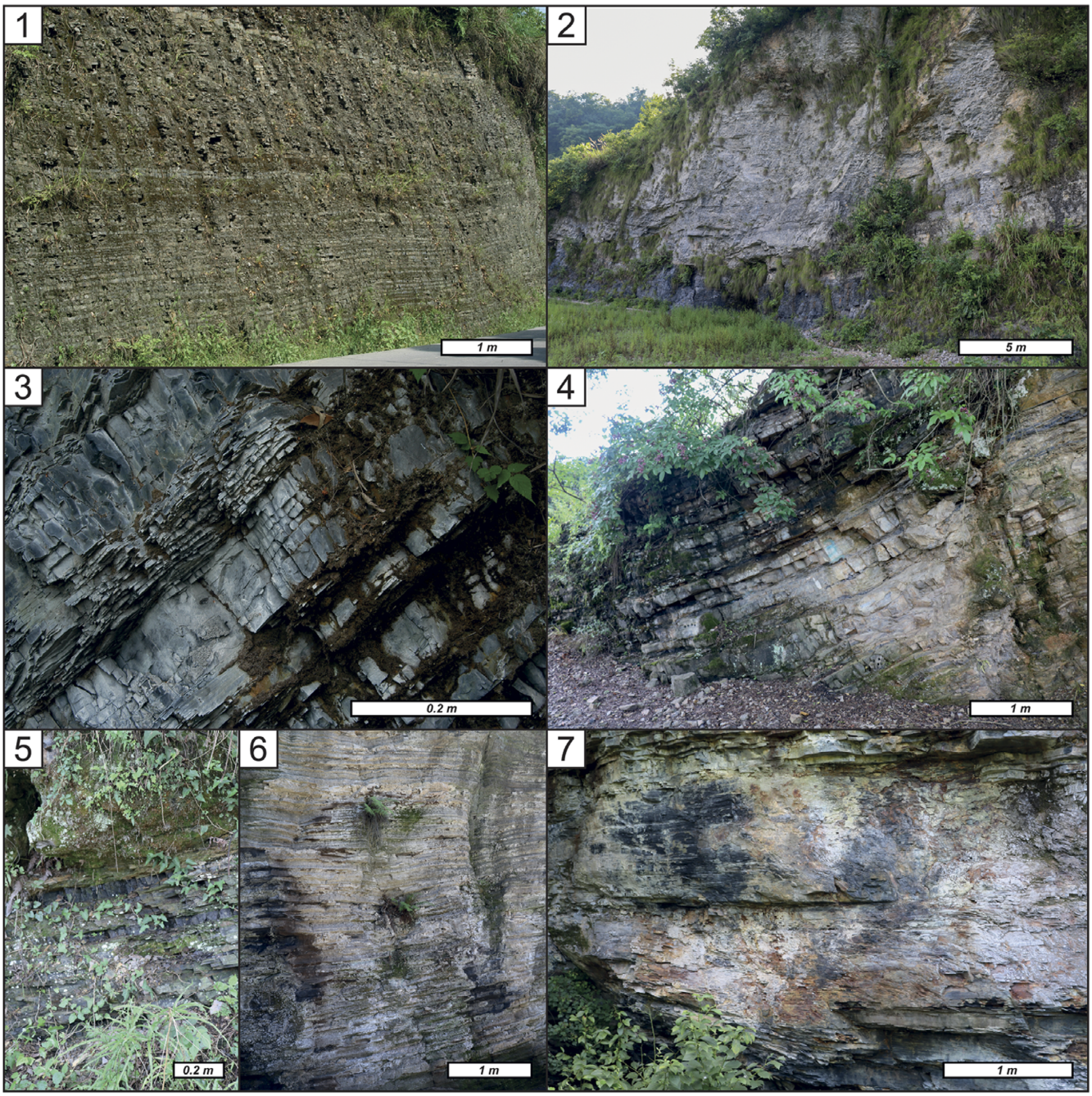



**Figure 3.** Representative field photographs of Ediacaran–Cambrian transition strata in South China. (**1**) Silicified shales of the uppermost 9 m of the Liuchapo Formation exposed at Yanwutan. (**2**) Boundary between dark-colored silicified shales of the Liuchapo Formation and overlying light-colored carbonates of the Dengying Formation at Sancha. (**3**) Silicified shales and mudstones of the lower Liuchapo Formation seen at Xugongping, 7 m above the base of the formation. (**4**) Member 1 of the Yanjiahe Formation at Jijiapo, comprising siliciclastic-rich, dolomitic mudstones and wackestones with associated thin chert beds. (**5**) Medium-bedded, AHC-bearing, phosphatic dolostones of Yanjiahe Formation Member 2 exposed at Jijiapo. (**6**) Thin mudstone layers interbedded with phosphatic and silicified wackestones and packstones, representing Yanjiahe Formation Member 3, observed at the Hezi'ao section. (**7**) Black shales of the basal Niutitang Formation at Sancha.

https://doi.org/10.1017/jpa.2026.10247 Published online by Cambridge University Press

the two (Fig. 2). Rare, silicified, microcrystalline lithoclasts occur in Unit 4 at Ganziping and Daping. Finally, Unit 5 (0.8–6 m thick) is dominated by silicified phosphatic wackestones and packstones. This unit is identifiable at the top of the Longbizui, Yanwutan, and Jianxincun sections.

Yanjiahe Formation. The Yanjiahe Formation is dominated by interbedded limestones and dolostones, with minor amounts of shale and chert. It was divided into five informal lithologic members by Guo et al. (2014, fig. 1) based on observations made at the Gunziao section (= Jijiapo section in this paper). The division of the Yanjiahe Formation into five distinct members is retained here; however, the diagnostic characteristics of each lithofacies are updated to reflect a broader range of sampled Yanjiahe Formation sections.

The basal member (6.8–11.5 m thick) is expressed as clay- and silt-rich massive dolomitic mudstones and wackestones associated with thin chert beds. This unit is observed at Jijiapo (Fig. 3.4) and Jiuqunao. It contains phosphatic grains (<300 μm) that co-occur with sparse peloids. The overall organic content is low, and no diagnostic microfossils are preserved in the lower part of the member. In the upper portion, simple plug-shaped trace fossils and AHC acritarchs have been reported (Ding et al., 1992; Dong et al., 2009; Guo et al., 2014; Ahn and Zhu, 2017; Chang et al., 2019).

Member 2 (Fig. 3.5) measures approximately 7.5–14.0 m in thickness. It is defined by organic-rich, silicified, phosphatic, dolomitic wackestones and packstones with interbedded phosphatic layers preserving microfossils characteristic of the AHC and *A. trisulcatus–P. anabarica* assemblage biozones (Dong et al., 2009; Guo et al., 2014; Ahn and Zhu, 2017). Abundant fossiliferous peloids (up to 400 μm), microbored grains, and scattered silicified lithoclasts are observable. Beds are mostly structureless, with only rare occurrences of weakly planar bedding.

Member 3 is recognized as 15–38 m of fossiliferous, phosphatic, silicified, lime wackestones and packstones interbedded with thin mudstone/siltstone (Fig. 3.6) and containing chert/phosphatic concretions. Peloids range in size from 40–200 μm. SSFs are observed in chert/phosphatic concretions. This facies is observed at Baiguotang, Jijiapo, Jiuqunao, and Hezi'ao.

Member 4 (1.0–5.0 m thick) is characterized by carbonaceous lime mudstones and wackestones. This facies always occurs after the first occurrences of acritarchs and SSFs. It is primarily observed at Hezi'ao, but also has been recorded at Jijiapo and Jiuqunao (Jiang et al., 2012).

Member 5, best seen at Jijiapo, is an approximately 2-m-thick dolostone with associated phosphatic clasts. Phosphatized animal embryos (Steiner et al., 2020), sarccorhytid ecdysozoan fossils (Wang et al., 2024), and SSFs characteristic of the *W. crosbyi* assemblage biozone (Guo et al., 2014, 2021) have been reported from this member.

Niutitang Formation. The basal unit of the Niutitang Formation, sampled at Sancha, Longbizui, and Taoying, may be recognized as a siliceous phosphoritic bed underlying a succession of organic-rich black shale (Fig. 3.7). In thin section, this bed is expressed as an organic-rich, peloidal, spicular shale hosting AHC assemblage microfossils. The section at Sancha consists of peloidal phosphatic shales displaying planar lamination to massive bedding, with occasional outsized chert lithoclasts. At all three localities, thin sponge spicule-rich bioclastic lenses occur within the Niutitang. A cm- to dm-thick metalliferous ore layer was observed in Niutitang outcrops at Sancha, Daping, and Taoying.

*Biostratigraphy.* The microfossil assemblages observed across the Ediacaran–Cambrian transition in South China represent multiple independent biotas comprising a variety of diverse organisms. Algae, cyanobacteria, and skeletal metazoans are identified, in addition to various organic remains of unknown biological affinities. Terminal Ediacaran successions are dominated by uniserial modular organisms of the HmNj assemblage (Fig. 4), which is succeeded by an array of early Cambrian AHC acanthomorphic acritarch taxa (Fig. 5) and SSFs (Fig. 6). At the five localities where both uniserial modular microfossils and acanthomorphic acritarchs are observed, the first occurrence of AHC acritarchs always postdates the last occurrence of HmNj assemblage taxa (Fig. 7).

HmNj assemblage zone. The HmNj assemblage zone is here defined as an acme biozone characterized by the abundant occurrence of *Horodyskia minor* and *Nenoxites jiumenensis* n. comb. in the terminal Ediacaran System. The uniserial modular microfossils *H. minor* (Fig. 4.1, 4.2) and *N. jiumenensis* (Fig. 4.3, 4.4) are recognized as strings of spherical (*H. minor*) or meniscate (*N. jiumenensis*) elements, which manifest in thin sections as circular and crescentic structures, respectively. The majority of *H. minor* and *N. jiumenensis* specimens are silicified. Some rare occurrences show limited pyritization, while others exhibit partial replacement by sub-parallel-oriented platy clay minerals.

*Horodyskia minor* specimens observed in thin section (Fig. 4.1, 4.2) consist of spheroidal to ellipsoidal beads with diameters of 0.1–0.8 mm. Total chain length varies with degree of disarticulation. Most specimens are observed as disarticulated chains or isolated spheroids randomly oriented within bedding planes; the latter can infrequently form hash deposits. Contact between individual beads is rare. Some exceptionally preserved specimens have quartz-pure haloes surrounding a string of beads (Fig. 4.1). Compared to *H. minor*, *N. jiumenensis* is more commonly preserved as multiple element chains (Fig. 4.3, 4.4). *Nenoxites jiumenensis* elements can be between 0.1–0.4 mm in diameter and, like in examples of *H. minor*, a halo of microcrystalline quartz may surround them.

The HmNj assemblage zone is recognized exclusively in shelf margin, slope, and basin deposits of the Liuchapo Formation (Fig. 7); no representatives of these taxa are found in the equivalent Ediacaran Dengying Formation deposited on the shelf. This is likely a consequence of taphonomic bias, as these bead-like microfossils are preserved via silicification of the rock succession in which they were deposited; this taphonomic pathway does not occur in the carbonates of the Dengying Formation. However, their absence could also reflect ecological exclusion from shallow-water environments during the latest Ediacaran.

Excluding the shallow water deposits (Jiuqunao, Jijiapo, Baiguotang, and Hezi'ao), HmNj assemblage zone fossils are identified in 8 of the 10 examined shelf margin to basin Liuchapo Formation sections (Fig. 7). At Ganziping, *H. minor* is found throughout the ~5.0 m section of the Liuchapo Formation, and *N. jiumenensis* is absent only from the uppermost 0.7 m. Both taxa occur throughout the ~5 m of exposed Liuchapo Formation at Daping. At Siduping, *H. minor* and *N. jiumenensis* are identified across a 10-m interval. *Horodyskia minor* is recognized between 4.0 and 48.0 m at Xugongping, with *N. jiumenensis* occurring over a similar range of 7.0–45.0 m. At Louyixi, *H. minor* is recognized between 9.5–15.0 m below the boundary between the Liuchapo and Niutitang formations, but only a single specimen of *N. jiumenensis* is documented at the stratigraphic depth of 12.5 m. At Longbizui, *H. minor* is observed throughout the lower 39.0 m of the Liuchapo Formation, whereas *N. jiumenensis* is limited to 7.0–13.0 m from the base of the

https://doi.org/10.1017/jpa.2026.10247 Published online by Cambridge University Press

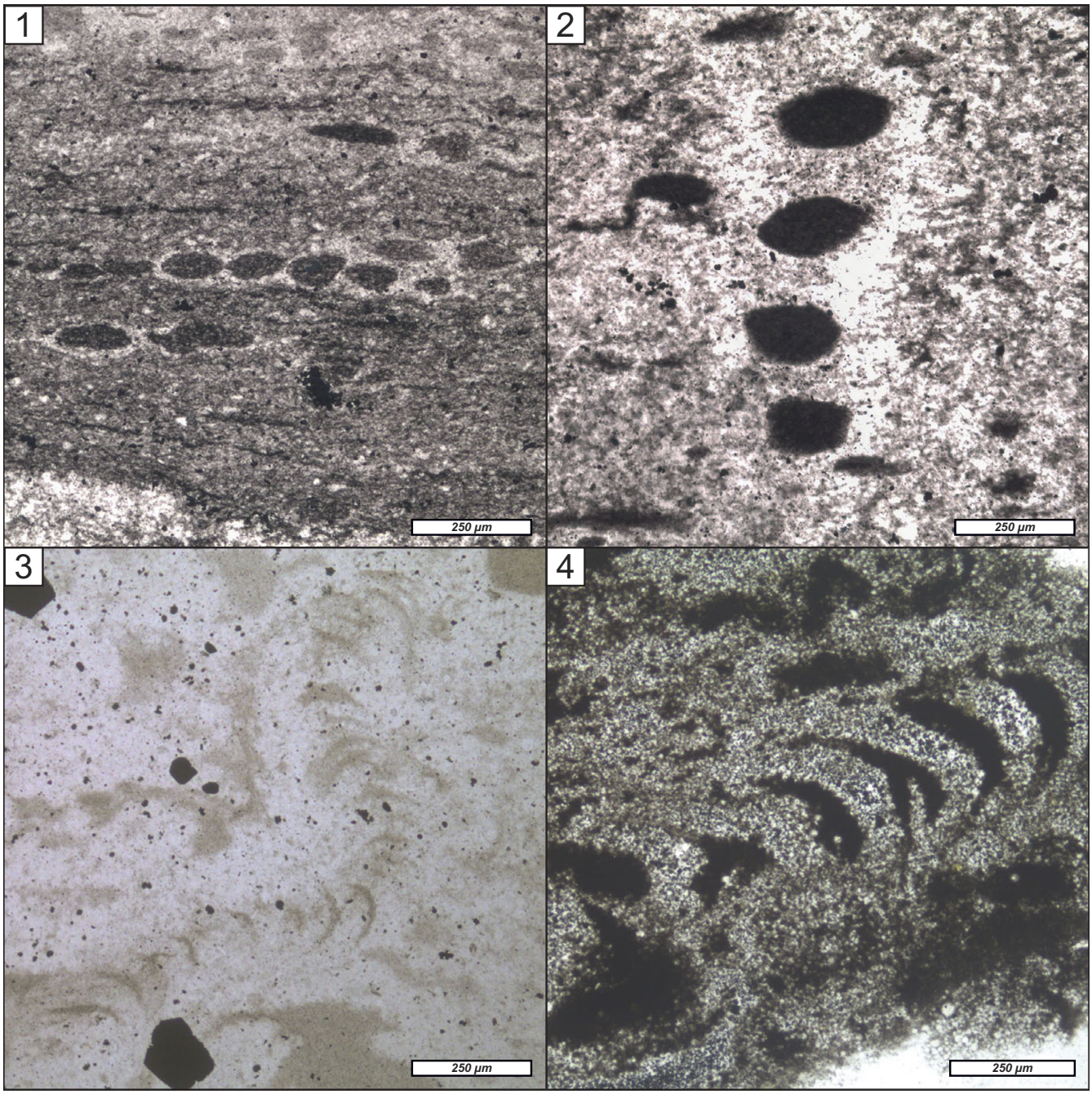



**Figure 4.** Transmitted light microscopic (TLM) images of representative HmNj (*Horodyskia minor–Nenoxites jiumenensis*) assemblage taxa. (**1**) *Horodyskia minor*, VPIGM–4828 (11-XGP-LCP-35.0, 19.3×141.0, H42/1), exhibiting quartz-rich halo surrounding string of beads. (**2**) *Horodyskia minor*, VPIGM–4829 (11-XGP-LCP-33.0, 21.1×126.8, F28/3). (**3**) *Nenoxites jiumenensis* n. comb., VPIGM–4830 (11-SDP-LCP-13.0, 119.0×8.0, T20/3). (**4**) *Nenoxites jiumenensis* n. comb., VPIGM–4831 (11-GZP-LCP-0.0, 21.7×128.0, E29/3), with terminal spherical segment (left of image). For this and other figures of TLM images, a VPIGM number is given for each image, followed by thin section number, Olympus BX-51 coordinates, and England Finder coordinates in brackets.

formation. *Horodyskia minor* and *N. jiumenensis* occur in a single sample from the basal 5 m of the Liuchapo Formation at Taoying. Both taxa are found throughout the lower 16.0 m of the Liuchapo Formation at the Jianxincun section. The highest absolute number of occurrences for both taxa typically occurs in the middle of the range across which they are present in each section. Neither *H. minor* nor *N. jiumenensis* are identified from the sections at Sancha, where the Liuchapo Formation was not sampled due to poor exposure, or Yanwutan, which preserves only AHC assemblage taxa (Fig. 7).

*Horodyskia minor* and *N. jiumenensis* do not occur with the same frequency throughout the sampled sections; the total number of identified *H. minor* specimens (1172) is almost three times that of the observed *N. jiumenensis* specimens (464). This may be a consequence of the increased disarticulation frequency of *H. minor* specimens. At Siduping, Xugongping, and Longbizui, the first

https://doi.org/10.1017/jpa.2026.10247 Published online by Cambridge University Press

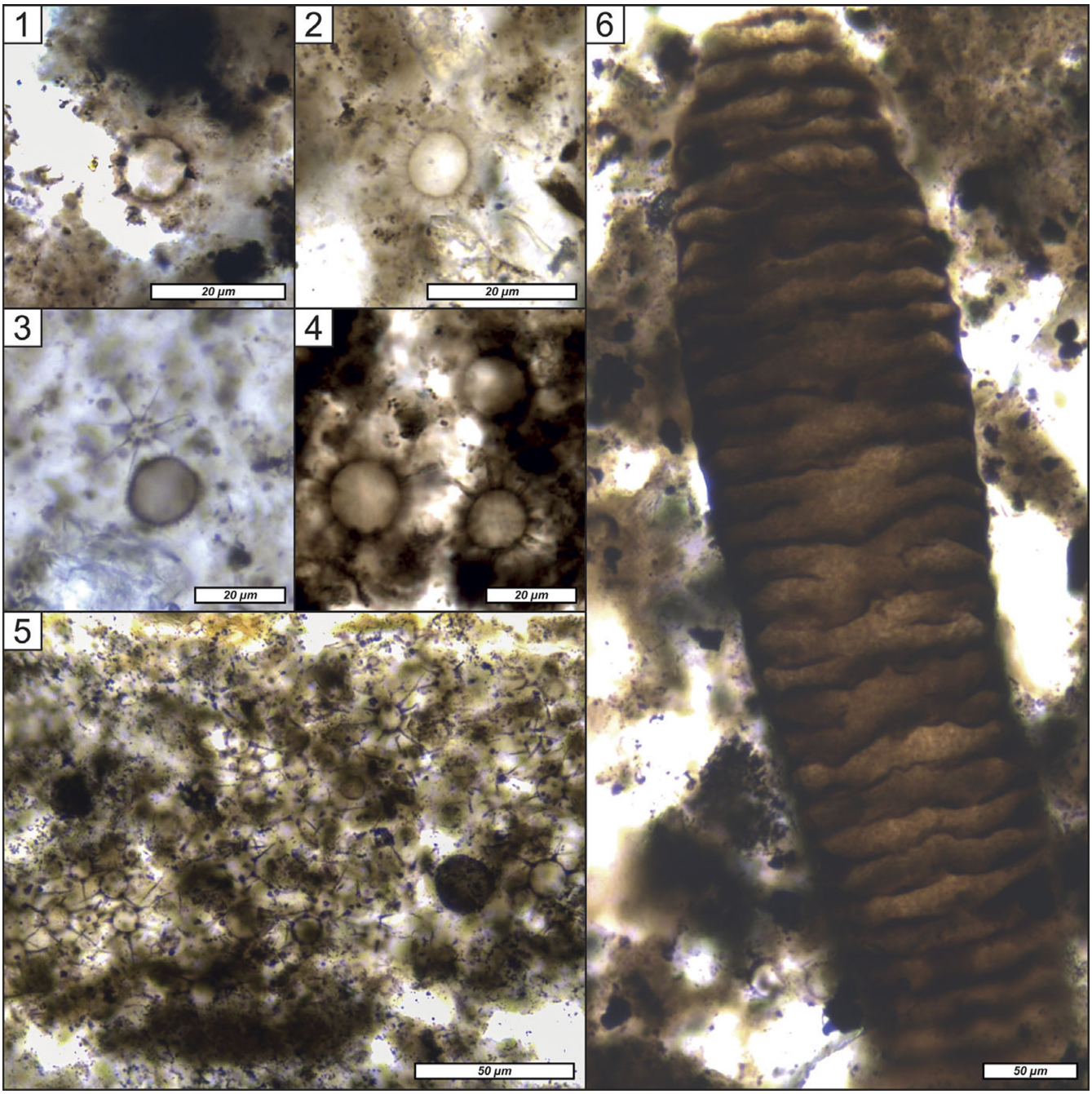



**Figure 5.** TLM images of representative AHC assemblage taxa. (**1**) *Asteridium tornatum*, VPIGM–4832 (JQN-YJH-10.4, 13.7×112.8, N13/4). (**2**) *Comasphaeridium annulare*, VPIGM–4833 (08JX-29.3, 13.3×129.8, O30/2). (**3**) *Heliosphaeridium ampliatum*, VPIGM–4834, at top of image, *Comasphaeridium annulare*, VPIGM–4835, at bottom (JQN-YJH-10.5, 4.8×121.5, W22/4). (**4**) Three specimens of *Heliosphaeridium ampliatum*, VPIGM–4836 to VPIGM–4838 clockwise from left specimen (08-HZA-Cam-5.4, 10.6×123.9, Q25/3). (**5**) Dense population of *Heliosphaeridium ampliatum* preserved within an organic-rich peloid, VPIGM–4839 (JQN-YJH-10.5, 23.4×124.8, D25/2). (**6**) *Megathrix longus* in association with *Heliosphaeridium ampliatum* (bottom left), VPIGM–4840 (11-BGT-YJH-0.9, 23.2×113.8, D15/1).

occurrence of *N. jiumenensis* postdates that of *H. minor*, while at Ganziping, Xugongping, and Longbizui, the last occurrence of *N. jiumenensis* predates that of *H. minor*. In only one section (Jianxincun) does *N. jiumenensis* occur in a thin section where *H. minor* is absent. Despite this, it is only at Longbizui that the occurrence range of these fossils is notably different within a succession.

Strata that contain *H. minor* and *N. jiumenensis* are dominated by these taxa; rarely are additional fossils identified within the assemblage. Organic-rich spheroidal forms, tens to hundreds of microns in diameter, are identified as *Chuaria circularis* Walcott, 1899; they co-occur alongside HmNj assemblage fossils throughout the documented stratigraphy. Rare sponge spicules are identified in the uppermost portions of the Liuchapo Formation at Ganziping, Xugongping, and Longbizui, where HmNj fossils are also present.

AHC assemblage zone. The AHC assemblage zone is characterized by the co-occurrence of three acanthomorphic acritarch taxa: *Asteridium tornatum*, *Heliosphaeridium ampliatum*, and

https://doi.org/10.1017/jpa.2026.10247 Published online by Cambridge University Press

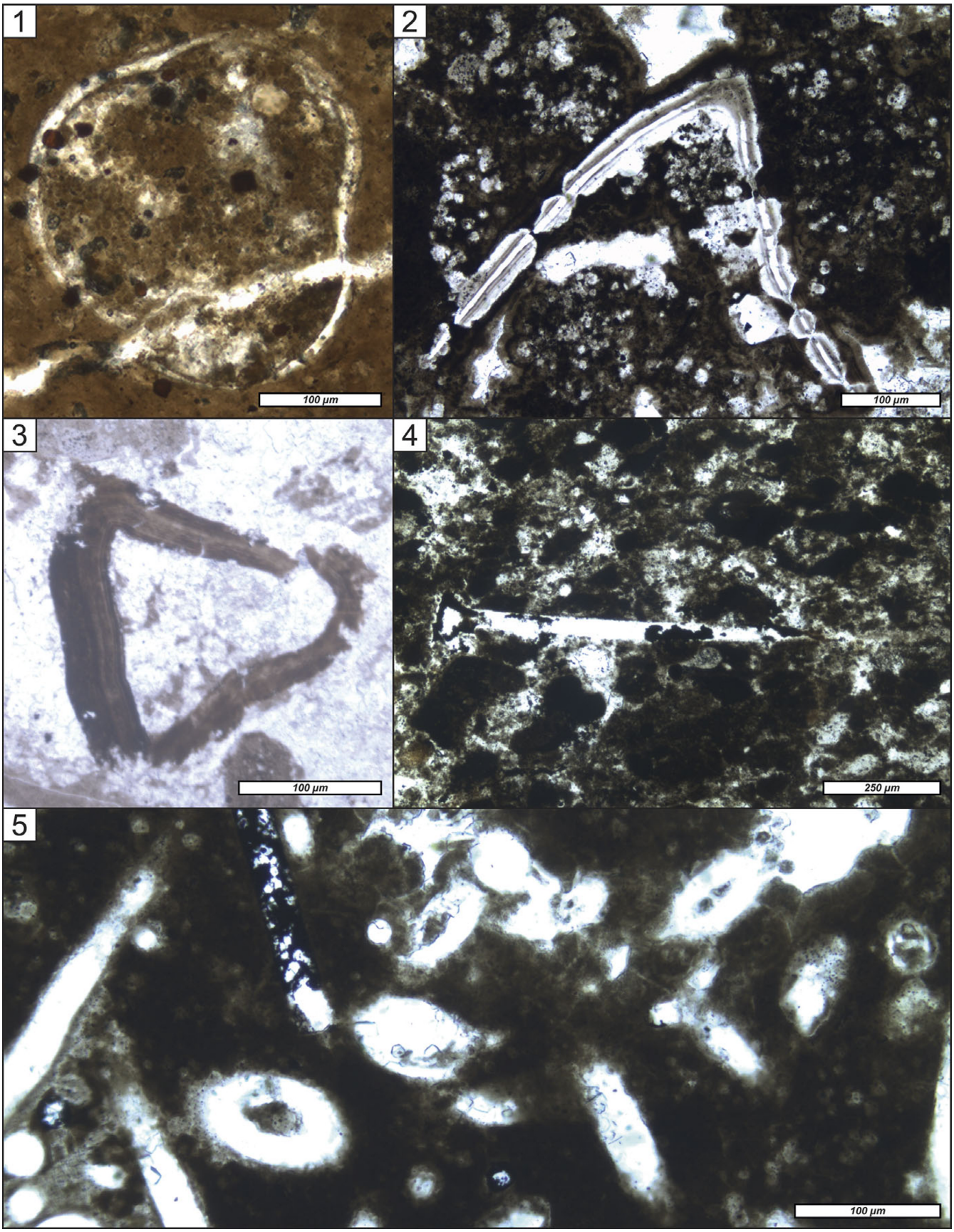



**Figure 6.** TLM images of SSFs identified in thin section, coincident with AHC assemblage acritarchs. (**1**) *Anabarites trisulcatus*, VPIGM–4841 (JPY-YJH-F-a, 5.4×126.1, W25/1). (**2**) *Kaiyangites novilis*, VPIGM–4842 (08-HZA-Cam-6.3, 17.8×126.4, J27/4). (**3**) *Protohertzina*? sp., VPIGM–4843 (11-BGT-YJH-0.01b, 10.1×125.4, R26/0). (**4**) *Zhijinites*? sp., VPIGM–4844 (08-HZA-Cam-5.8, 6.5×140.0, U41/3). (**5**) Sponge spicules, VPIGM–4845 (08-HZA-Cam-6.0, 16.5×142.8, K43/4). Most are monaxons, but the specimen ~1/3 from the right appears to be a hexactine.

https://doi.org/10.1017/jpa.2026.10247 Published online by Cambridge University Press

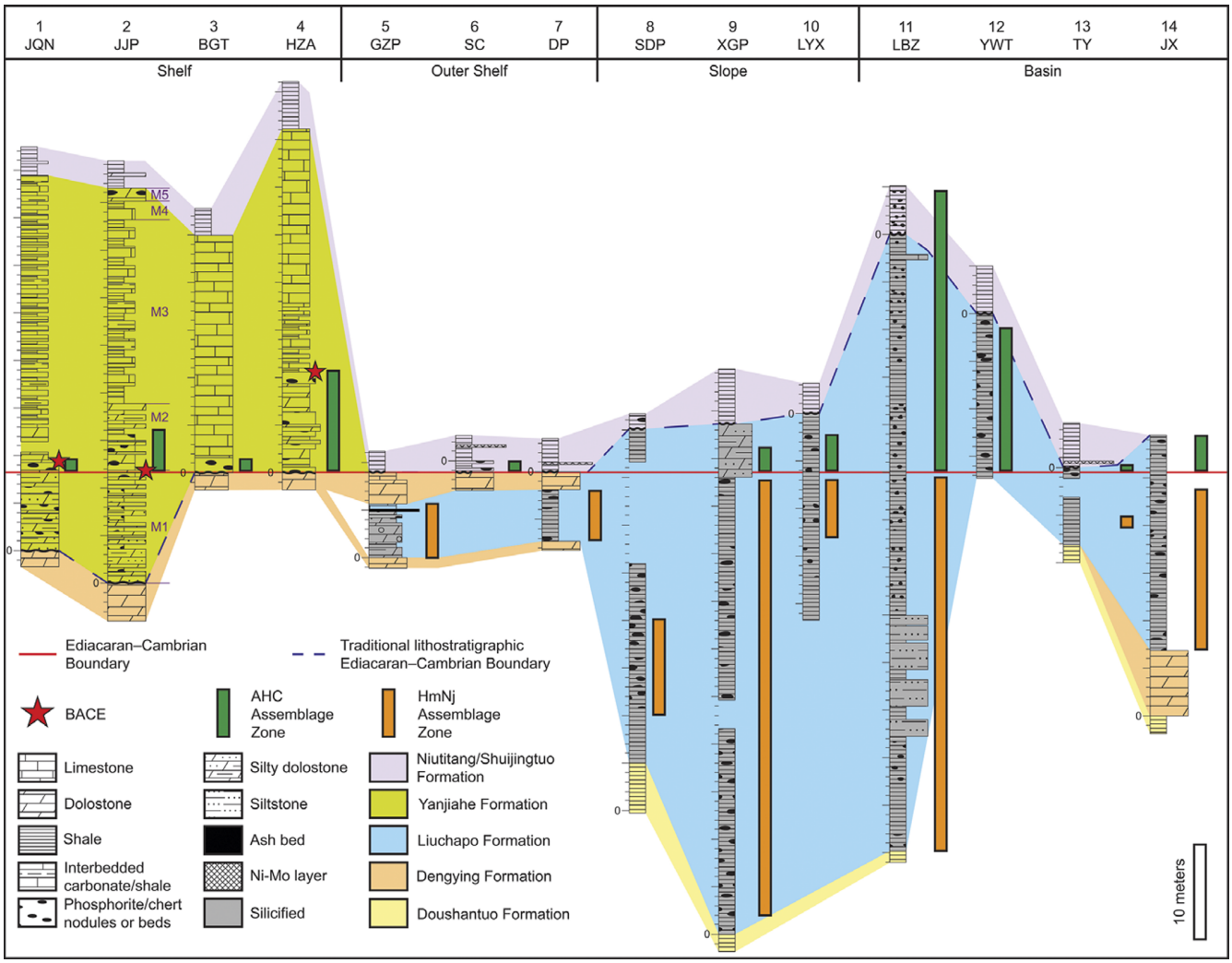



**Figure 7.** Ediacaran–Cambrian stratigraphic relationships and biostratigraphy of the Yangtze Craton. Stratigraphic columns for each studied locality are plotted against the occurrences of the HmNj (*Horodyskia minor–Nenoxites jiumenensis*) assemblage (orange bars) and AHC (*Asteridium–Heliosphaeridium–Comasphaeridium*) assemblage (green bars) zones. Using the last and first occurrences of these assemblage zones, the Ediacaran–Cambrian boundary (red line) can be defined throughout the shelf-to-basin transect represented by the Yangtze Craton stratigraphy. The boundary is placed at the stratigraphic horizon containing the first occurrence of AHC taxa. HmNj assemblage zone taxa provide a maximum constraint on the boundary. Traditionally, the boundary (purple dashed line) has been placed at the top of the Dengying and Liuchapo formations (e.g., Xiang et al., 1999). Occurrences of the BACE (BAsal Cambrian Isotope Excursion) are based on published data: Jiuqunao (Jiang et al., 2012), Jijiapo (Jiang et al., 2012; Ahn and Zhu, 2017), Hezi'ao (Jiang et al., 2012). Stratigraphic heights or depths are marked in meters, with the zero-tick mark representing the datum from which sections were measured in the field. The stratigraphic gap in the Liuchapo Formation at Taoying is approximate due to the sample from the basal Liuchapo being collected from the nearby Wenghui section. Sample abbreviations at top match those in Figure 1: JQN = Jiuqunao; JJP = Jijiapo (M1–M5 mark the five lithostratigraphic members of the Yanjiahe Formation recognized at this section); BGT = Baiguotang; HZA = Hezi'ao; GZP = Ganziping; SC = Sancha; DP = Daping; SDP = Siduping; XGP = Xugongping; LYX = Louyixi; LBZ = Longbizui; YWT = Yanwutan; TY = Taoying; JX = Jianxincun.

*Comasphaeridium annulare*. As initially defined by Yao et al. (2005), the lower limit of the assemblage zone was set at the abundant occurrence of *A. tornatum* and *H.* cf. *lubomlense* or *H. ampliatum*, with *C. annulare* occurring at roughly the same level but in lower abundance, and its upper limit was marked by the first appearance of the acritarch genus *Skiagia* Downie, 1982. Based on subsequent studies (Dong et al., 2009; Ahn and Zhu, 2017; Luo and Zhu, 2025) and a regional survey presented in this paper, we propose a modified definition of the AHC assemblage zone: its lower limit at the first occurrence of an AHC taxon, its duration characterized by abundant occurrence of the AHC taxa, and its upper limit at the last occurrence of the AHC taxa, which are thought to predate the first appearance of *Skiagia*.

The AHC taxa have relatively small vesicle diameters (~5–20 μm) but exhibit distinctive process morphologies. Specimens of *A. tornatum* are identified by evenly distributed solid, short, and conical processes with pointed tips (Fig. 5.1). *Heliosphaeridium ampliatum* (Fig. 5.3–5.5) has much longer processes than those of *A. tornatum*, with process lengths often equaling or exceeding the diameter of the vesicle, but they have an overall conical morphology. Examples of *C. annulare* (Fig. 5.2) commonly have larger vesicle sizes than either *A. tornatum* or *H. ampliatum* and a different process morphology; *C. annulare* processes are short, numerous, and densely distributed, creating hair-like projections outwards from the vesicle.

In most cases, AHC microfossils occur in high abundance (e.g., ~20–50 specimens per thin section). The majority of the identified

https://doi.org/10.1017/jpa.2026.10247 Published online by Cambridge University Press

acritarchs, particularly *H. ampliatum*, are observed as clusters of many individuals (Fig. 5.5), although they can be found individually. AHC acritarchs are typically recovered from siliceous and phosphatic peloidal wackestones and packstones, frequently within peloids, but can also be preserved in silicified mudstones. The AHC assemblage zone is identified in 11 of the 14 studied sections and is represented across the shelf-to-basin transect (Fig. 7).

Among the AHC acanthomorphic acritarchs, *H. ampliatum* is by far the most abundant in this study (1523 individuals). This is primarily a result of the preservation of entire populations of *H. ampliatum* within organic-rich peloids (Fig. 5.5). In some instances, *H. ampliatum* reaches population densities of several hundred individuals per square centimeter in thin section. *Heliosphaeridium ampliatum* is the AHC acritarch most prone to degradation, particularly those individuals preserved within peloids, with specimens commonly exhibiting at least some broken processes and varying degrees of damage to vesicle walls; occasionally, isolated broken processes may be observed. This degradation can be challenging for classification, because *H. ampliatum* individuals with broken processes can resemble *A. tornatum*. However, if the processes were broken, they would have a truncated distal end instead of the pointed tip characteristic of *A. tornatum*, and the differential density of the processes would still be discernible; additionally, *H. ampliatum* is recognized as having hollow processes, whereas those of *A. tornatum* are solid. Specimens outside of peloids are solitary and usually undamaged. *Heliosphaeridium ampliatum* is preserved across the entire shelf-to-basin transect. In shelf successions, *H. ampliatum* is recovered from the lower Yanjiahe Formation at Jiuqunao, Jijiapo, Baiguotang, and Hezi'ao. Within the slope and basin, this taxon occurs in the lower Niutitang phosphorite at Sancha and Longbizui, as well as in the uppermost Liuchapo Formation at Xugongping, Louyixi, Longbizui, Yanwutan, and Jianxincun.

*Comasphaeridium annulare* is the second most abundant AHC acritarch; however, the total number of recovered specimens (151) is only a tenth of the number of identified *H. ampliatum*. Single *C. annulare* microfossils can occur in close aggregation with populations of *H. ampliatum* inside peloids, but generally they are found as isolated individuals in the matrix of peloidal wackestones and packstones. Of the three AHC taxa, *H. ampliatum* and *C. annulare* are most frequently observed together in thin section; of the sections where *H. ampliatum* is recovered, only the Yanjiahe Formation at Baiguotang does not also contain *C. annulare*. Like *H. ampliatum*, *C. annulare* occurs across the shelf-to-basin transect. Specimens are recovered from shelf sections represented by the lower Yanjiahe Formation at Jiuqunao, Jijiapo, and Hezi'ao. Within the shelf margin, slope, and basin deposits, *C. annulare* is identified from the uppermost Liuchapo Formation at Xugongping, Louyixi, Longbizui, Yanwutan, and Jianxincun. Additionally, *C. annulare* occurs in the lowermost Niutitang Formation at Sancha, Longbizui, and Taoying.

*Asteridium tornatum* is the rarest of the three AHC acritarch taxa, with only 78 individuals identified. Specimens are frequently observed as individuals, but can occur in groups of two or three. Like *H. ampliatum*, this taxon is commonly associated with organic-rich peloids. Despite their limited numbers, *A. tornatum* is recognized across the shelf-to-basin transect. The shelf deposits of the lower Yanjiahe Formation at Jiuqunao, Jijiapo, and Hezi'ao contain *A. tornatum*. In shelf margin, slope, and basin deposits, this taxon is recovered from the Niutitang Formation at Sancha and the Liuchapo Formation at Longbizui and Yanwutan.

Overall diversity is much higher within the AHC assemblage zone compared to the HmNj assemblage zone, with several additional taxa recorded in association with the AHC acritarchs across the Yanjiahe, Niutitang, and Liuchapo formations (see supplementary Systematic Paleontology for additional details). *Megathrix longus* (Fig. 5.6) is a long, tubular microfossil exhibiting evenly spaced corrugated or curved cross walls within each tube, possibly representing a species of oscillatoriacean cyanobacteria (Shang et al., 2016). *Megathrix longus* is frequently associated with AHC assemblage zone taxa (Yao et al., 2005; Dong et al., 2009) and is thus a useful additional biostratigraphic indicator for the zone. Sponge spicules (Fig. 6.5) are frequently observed, as well as relatively rare examples of fragmented SSFs (Fig. 6.1–6.4).

Several other acritarch species co-occur with the AHC taxa. Additional species of *Heliosphaeridium*, *H. coniferum* (Downie, 1982) Moczydłowska, 1991 (Fig. 8.1) and *H. lubomlense* (Kirjanov, 1974) Moczydłowska, 1991 (Fig. 8.2), are recognized, as well as the potential green microalga *Yurtusia uniformis* Dong et al., 2009 (Fig. 8.5; see also Dong et al., 2009; Shang et al., 2020). *Heziaosphaera bimorphospina* n. gen. n. sp. (Fig. 8.3, 8.4), which exhibits process morphologies characteristic of both *Heliosphaeridium ampliatum* and *C. annulare*, was also discovered within the Yanjiahe Formation at Hezi'ao. Recovered specimens of *Archaeophycus yunnanensis* (Song in Luo et al., 1982) Dong et al., 2009 are identifiable as cuboidal cell colonies forming dyads, triads, and tetrads (Fig. 8.6). Examples of *Chuaria circularis* Walcott, 1899 preserved as unbroken but deformed outer envelopes (Fig. 8.7; see also Steiner, 1996), co-occur with the acanthomorphic acritarchs throughout the documented stratigraphy. Similar fossils from the basal Cambrian in South China have been described as filmy fossils (Luo and Zhu, 2025) and interpreted as cuticular remains of early animals (Yin et al., 2017).

Other fossils. Thirty-eight SSFs were identified in thin section during this study. These specimens occur in the Yanjiahe Formation at Baiguotang and Hezi'ao, and in the Liuchapo Formation at Yanwutan and Jianxincun. They were recovered from the same horizons as the AHC assemblage zone taxa, generally coincident with or postdating the first occurrence of these acritarch species. Despite many specimens being identified, only a few may be confidently assigned taxonomically. Numerous challenges, including the fragmentary nature of the fossils and the difficulty associated with recognizing diagnostic features in thin section, mean it is not possible to define the taxonomic affinities for the majority of the SSF material; however, eight specimens can be assigned to pre-existing SSF taxa (see also supplementary Systematic Paleontology).

Two specimens of *Anabarites trisulcatus* Missarzhevsky in Voronova and Missarzhevsky, 1969 (Fig. 6.1) are identified from the Yanjiahe Formation exposed at Jijiapo and Hezi'ao. *Anabarites trisulcatus* forms part of the *A. trisulcatus–P. anabarica* assemblage zone, which defines the basal boundary of the Cambrian System in South China (Steiner et al., 2004, 2007, 2020). The Hezi'ao specimen was recovered from the 0.2-m interval of the Yanjiahe Formation, coincident with the first appearance of AHC taxa within this section. The co-occurrence of these taxa lends support to the inference that the AHC assemblage may be correlated with the *A. trisulcatus–P. anabarica* assemblage zone (Yao et al., 2005; Ahn and Zhu, 2017). The Jijiapo specimen, recovered from a float sample, has limited biostratigraphic utility because its precise stratigraphic position is uncertain. The most abundant identifiable SSF is *Kaiyangites novilis* Qian and Yin, 1984 (Fig. 6.2), an eponymous fossil in the *P. anabarica–K. novilis* assemblage zone (Steiner et al., 2007). Four specimens of *K. novilis* occur in the first 1.2 m of the

https://doi.org/10.1017/jpa.2026.10247 Published online by Cambridge University Press

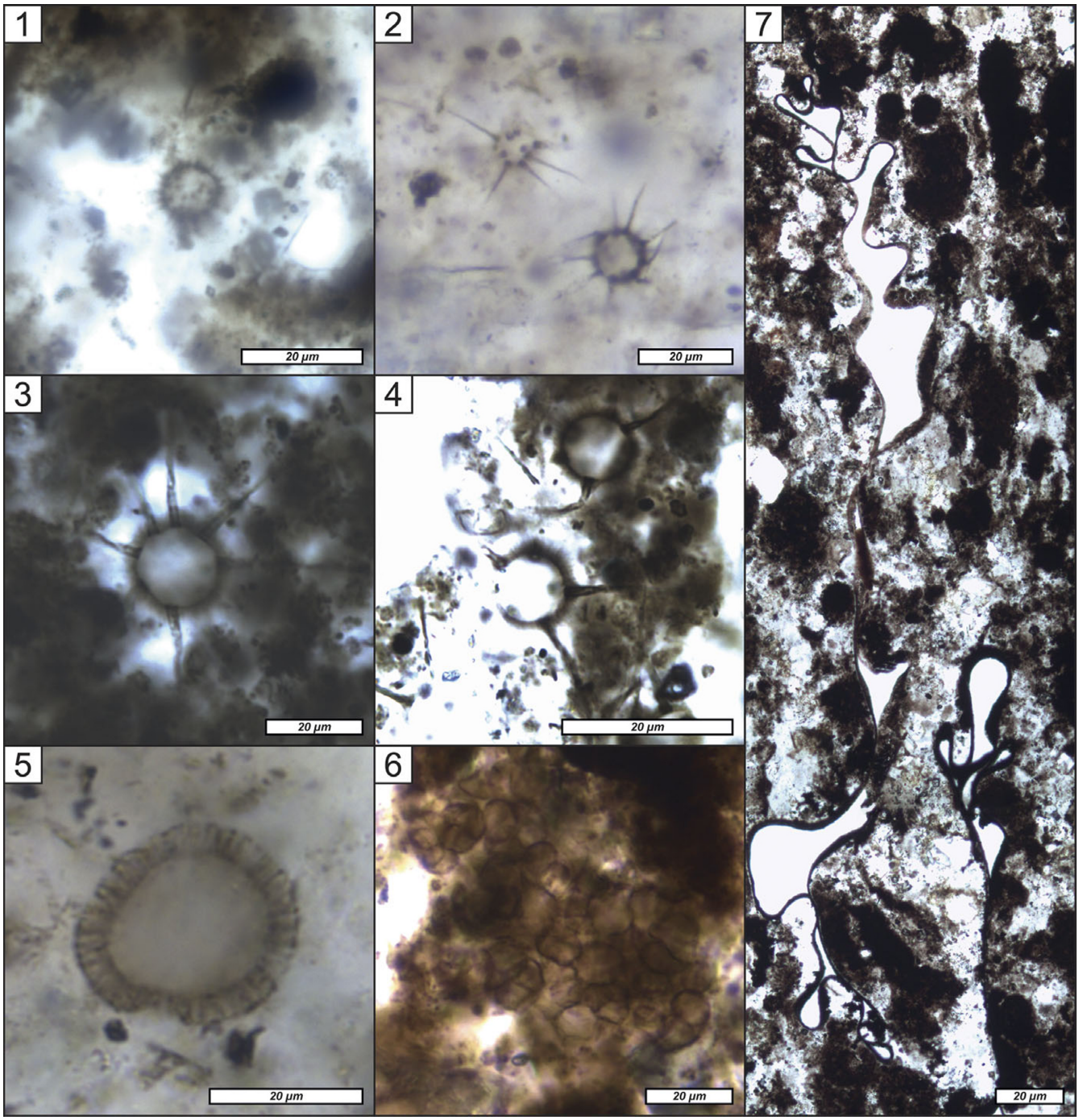



**Figure 8.** TLM images of additional microfossils identified in association with AHC (*Asteridium–Heliosphaeridium–Comasphaeridium*) taxa. (**1**) *Heliosphaeridium coniferum*, VPIGM–4846 (08-HZA-Cam-5.2, 16.7×122.7, K23/4). (**2**) *Heliosphaeridium lubomlense* at bottom of image, VPIGM–4847; *Heliosphaeridium ampliatum* at top, VPIGM–4848 (JQN-YJH-10.5, 4.2×133.1, X34/1). (**3**) *Heziaosphaera bimorphospina* n. gen. n. sp., holotype, VPIGM–4849 (08-HZA-Cam-6.3, 7.0×146.5, U47/0). (**4**) Two specimens of *Heziaosphaera bimorphospina* n. gen. n. sp., VPIGM–4849 (08-HZA-Cam-6.3, 6.1×147.1, W48/3). (**5**) *Yurtusia uniformis*, VPIGM–4850 (JQN-YJH-10.5, 6.8×106.0, U7/3). (**6**) *Archaeophycus yunnanensis* population, VPIGM–4851 (08JX-31.0, 15.8×129.9, L31/3). (**7**) A large *Chuaria circularis* envelope. A second partial envelope is visible in the lower right of the image, VPIGM–4853 (11-HZA-YJH-22.1, 11.9·110.0, P11/3).

Yanjiahe Formation at Baiguotang, while a further two are identified within the 6.3-m interval of the Yanjiahe Formation at Hezi'ao. Both of these *K. novilis* occurrence intervals are coincident with AHC assemblage zone taxa.

Sponge spicules (Fig. 6.5) are recognized across the shelf-to-basin transect, occurring in the Yanjiahe Formation at Jiuqunao, Jijiapo, Baiguotang, and Hezi'ao; in the Liuchapo Formation at Ganziping, Xugongping, Louyixi, Longbizui, Yanwutan, and Jianxincun; and in the Niutitang Formation at Sancha, Siduping, Longbizui, and Taoying. At several localities, the first occurrence of sponge spicules predates that of AHC acritarchs, with slope and basin sections demonstrating co-occurrence of sponge spicules and

https://doi.org/10.1017/jpa.2026.10247 Published online by Cambridge University Press

HmNj taxa (see also Chen et al., 2023). Spicules are typically monaxonal monactine or diactine. Hexactine spicules are infrequently observed. Monaxonal monactine spicules have one axis and one ray, with one end of the spicule pointed, while the opposite end is rounded. Monaxonal diactines are similarly defined by a single axis but have two rays, resulting in a morphology in which both spicule ends are pointed. Archetypal hexactine spicules have three orthogonal axes and six rays. However, one or two rays may be aborted, resulting in modified pentactines or stauractines, with five or four rays, respectively. Spicules are typically preserved as casts (Fig. 6.5). In addition to the spicules recorded in thin section, pyritized sponge body fossils and spicules up to several centimeters in length were observed in shale slabs of the Niutitang Formation at Siduping (Fig. 9.1).

At Yanwutan, macroscopic carbonaceous compressions (Fig. 9.2–9.4), interpreted as macroalgae, were identified within a stratigraphic interval of the upper Liuchapo Formation approximately 8–12 m below the Liuchapo–Niutitang boundary, preserved in layers of silty shale intercalated with thin-bedded carbonaceous limestone. These macroalgal fossils are probably vendotaenids, although they lack the longitudinal striae characteristic of the genus *Vendotaenia* Gnilovskaya, 1971, and some specimens exhibit transverse annulations (Fig. 9.4). Vendotaenids have also been described from the Yanjiahe Formation at Jijiapo (Guo et al., 2008). At both localities, these vendotaenids are generally preserved with high density. Additionally, Guo et al. (2012) reported the macroalgal fossil *Protoconites minor* Chen et al., 1994, and the problematic macrofossil genus *Yanjiahella* Guo et al., 2012, from the Yanjiahe Formation at Jijiapo; *Yanjiahella* has been interpreted as an echinoderm (Guo et al., 2012; Topper et al., 2019), although this has been disputed (Zamora et al., 2020).

## Discussion

The GSSP for the Cambrian is defined at a point within the Chapel Island Formation at Fortune Head, Newfoundland (Narbonne et al., 1987). The stratigraphic position of the GSSP is coincident with the first appearance (at the time of ratification) of the trace fossil *T. pedum*, which symbolizes the first widespread occurrence of diverse, abundant, complex trace fossils that likely reflects a major metazoan behavioral shift (Geyer and Uchman, 1995; Narbonne et al., 1987; Geyer, 2005). Thus, global correlation of the Ediacaran–Cambrian boundary, as currently defined, depends on recognizing the first appearance of *T. pedum* (Landing, 1994; Peng et al., 2012).

However, there are limitations associated with using *T. pedum* as the GSSP for the Ediacaran–Cambrian boundary (Babcock et al., 2014). At a global scale, the first appearance of *T. pedum* is highly variable relative to other potential markers (Topper et al., 2022), and it can occur coincident with fossils that are traditionally regarded as either Ediacaran or Cambrian taxa (e.g., Buatois, 2018). It has further been argued that *T. pedum* is largely restricted to shallow marine environments or transgressive regimes (Geyer, 2005) and occurs only within coarser siliciclastic facies (Wilson et al., 2012; Buatois et al., 2013). As a result of this facies

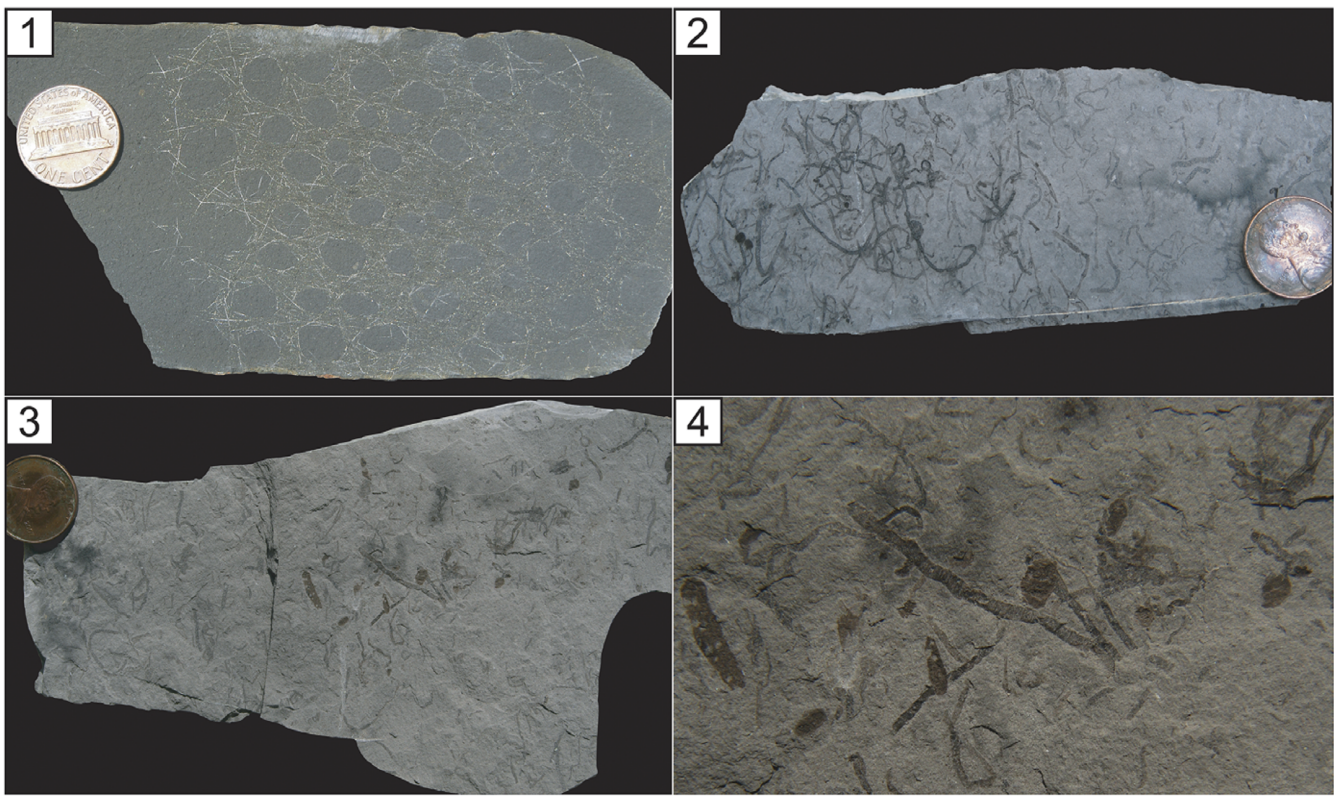



**Figure 9.** Cambrian macrofossils from the Niutitang and Liuchapo formations. (**1**) Pyritized sponge body fossil from Niutitang Formation shales at Siduping. Field photograph. (**2–4**) Vendotaenid-type macroalgae and putative metazoan carbonaceous compressions from the Liuchapo Formation at Yanwutan. Field photographs. (**4**) Enlarged view of (**3**), highlighting a ribbon-like fossil exhibiting transverse striations. Width of one cent coin = 1.9 cm.

https://doi.org/10.1017/jpa.2026.10247 Published online by Cambridge University Press

dependence, it is challenging to accurately calibrate the first occurrence of *T. pedum* against other commonly used boundary approximations, such as carbon isotope chemostratigraphy and SSF occurrences, which have been used independently to approximate and correlate the Ediacaran–Cambrian boundary and earliest Cambrian strata in carbonate-dominated successions (Maloof et al., 2010; Yang et al., 2016; Steiner et al., 2020; Guo et al., 2021; Luo et al., 2024).

Acanthomorphic acritarchs have emerged as an additional global biostratigraphic marker for the beginning of the Cambrian (Yao et al., 2005; Dong et al., 2009; Ahn and Zhu, 2017; Zhu and Li, 2017). Basal Cambrian acanthomorphic acritarchs have previously been used in biostratigraphic correlation between the stratigraphy of the East European Platform and Cambrian successions worldwide, with four assemblage zones developed based on characteristic co-occurring acritarch morphologies (Moczydłowska, 1991). Microfossils belonging to the first of these assemblage zones, defined by the co-occurrence of *Asteridium tornatum* and *Comasphaeridium velvetum* Moczydłowska, 1988 (Moczydłowska, 1991), and their equivalents (e.g., Yao et al., 2005), have been recovered in Avalonia (Palacios et al., 2011), the Lesser Himalaya (Tiwari, 1999), South Australia (Moczydłowska and Zang, 2006), Spain (Palacios and Vidal, 1992), Kazakhstan (Sergeev and Ogurtsova, 1989), Tarim (Yao et al., 2005; Dong et al., 2009), and South China (Yin, 1987a, b; Ding et al., 1992; Zang, 1992; Yao et al., 2005; Dong et al., 2009; Ahn and Zhu, 2017). These acritarchs may therefore have a global distribution, are morphologically distinctive, and temporally constrained, indicating their global biostratigraphic potential for identifying the Ediacaran–Cambrian boundary (Ahn and Zhu, 2017).

In South China, the first early Cambrian acanthomorphic acritarch assemblage zone, equivalent to the *A. tornatum–C. velvetum* zone established by Moczydłowska (1991), comprises the morphologically distinct *A. tornatum*, *H. ampliatum*, and *C. annulare* (Yao et al., 2005). This assemblage zone has been recognized in multiple stratigraphic successions across the Yangtze and Tarim cratons (Yao et al., 2005; Dong et al., 2009; Ahn and Zhu, 2017; Luo and Zhu, 2025; this study).

As originally defined, the AHC assemblage zone was marked by the abundant occurrence of an AHC taxon at its lower limit and the first appearance of the acritarch genus *Skiagia* at its upper limit (Yao et al., 2005). This definition implies that the AHC assemblage zone spans the entire Terreneuvian Series, although AHC taxa are only known from Stage 1 and have not been documented in Stage 2. New data presented here and published elsewhere (Dong et al., 2009; Ahn and Zhu, 2017; Luo and Zhu, 2025) allow us to refine the definition of the AHC assemblage zone, with its lower limit at the first occurrence of an AHC taxon, its duration characterized by abundant occurrence of the AHC taxa, and its upper limit at the last occurrence of the AHC taxa. The redefined AHC assemblage zone is likely Fortunian in age, given that the AHC assemblage zone underlies the *W. crosbyi* assemblage biozone in the Yanjiahe Formation at Jijiapo (Guo et al., 2014, 2021). The *W. crosbyi* assemblage zone has been proposed to mark the basal boundary of Cambrian Stage 2 (Peng et al., 2020; Steiner et al., 2020). Thus, the refined AHC assemblage zone is restricted to Stage 1, much narrower in stratigraphic scope than the original definition. Future studies are required to fill the biostratigraphic gap between the AHC assemblage zone and the first appearance of *Skiagia*.

This study expands the number of Yangtze Craton successions where AHC acritarchs are identified (Figs. 1.2, 7). AHC assemblage zone taxa are recovered from 11 of the 14 analyzed sections (Fig. 7): Jiuqunao, Jijiapo, Baiguotang, Hezi'ao, Sancha, Xugongping, Louyixi, Longbizui, Yanwutan, Taoying, and Jianxincun. These deposits represent a complete transect across the shelf-to-basin transition of the Yangtze Craton. AHC acritarchs are recognized in all represented depositional environments on the craton, occurring in the Liuchapo, Yanjiahe, and Niutitang formations within siliceous and phosphatic mudstones, wackestones, packstones, and shales.

AHC acritarchs co-occur with *Anabarites trisulcatus*, representative of the first SSF assemblage zone recognized in South China, supporting previous conclusions regarding the correlation between the AHC assemblage zone and this SSF zone (Ahn and Zhu, 2017). Previously published carbon isotope and radiometric age data for the Jiuqunao (Jiang et al., 2012), Jijiapo (Jiang et al., 2012; Ahn and Zhu, 2017), Hezi'ao (Jiang et al., 2012), and Longbizui (Wang et al., 2012; Guo et al., 2013) sections demonstrate that the AHC assemblage zone consistently occurs in close proximity to a pronounced negative carbon isotope excursion interpreted to represent the BACE (Fig. 7). Consequently, the first occurrence of AHC assemblage zone taxa throughout the Yangtze Craton can be correlated with both SSF and geochemical approximations for the Ediacaran–Cambrian boundary, indicating that these microfossils provide a consistent and reliable way to identify the boundary (Ahn and Zhu, 2017; Zhu and Li, 2017; Chang et al., 2025) across a variety of depositional environments and preservational settings (Fig. 7).

The identification of *K. novilis* alongside diagnostic AHC taxa provides additional support for the proposed correlation between the AHC and *A. trisulcatus–P. anabarica* assemblage zones (Ahn and Zhu, 2017). *Kaiyangites novilis* is a diagnostic fossil in the *P. anabarica–K. novilis* assemblage zone (Steiner et al., 2007), considered a deep-water equivalent to the *A. trisulcatus–P. anabarica* assemblage zone. *Anabarites trisulcatus* is restricted to shallow water limestone or dolostone sequences, whereas *K. novilis* was considered to be limited to siliceous and limestone beds deposited in deeper water beyond the shelf (Steiner et al., 2007). The occurrences of *K. novilis* in shallow water settings at Baiguotang and Hezi'ao expand the environmental distribution of this taxon, although it remains a rare SSF in shelf deposits, and confirms the equivalence of the two SSF assemblage zones. Consequently, both the *A. trisulcatus–P. anabarica* and *P. anabarica–K. novilis* assemblage zones remain useful for correlating across early Cambrian deposits in China and may also be regarded as coincident with the AHC assemblage zone.

The stratigraphic position of the Ediacaran–Cambrian boundary, as recognized by the first occurrence of AHC assemblage zone taxa, fluctuates across the Yangtze Craton relative to lithostratigraphic boundaries (Figs. 2, 7). In the shelf, the boundary, defined by the lowest stratigraphic occurrences of AHC biozone taxa, occurs in the lower Yanjiahe Formation; however, the precise location shows notable variability. At Jiuqunao and Jijiapo, the first occurrence of AHC taxa is around the boundary between members 1 and 2 of the Yanjiahe Formation, 10–20 m above the lower boundary of the formation (Fig. 7). At Baiguotang and Hezi'ao, AHC taxa first appear directly above the boundary between the Dengying and the Yanjiahe formations (Fig. 7) due to more substantial erosional unconformities in these sections. In the shelf margin, the Ediacaran–Cambrian boundary is best placed in the basal Niutitang Formation, where the AHC assemblage biozone is identified at the Sancha section (Fig. 7). In the slope and basin, the boundary again shows variability relative

https://doi.org/10.1017/jpa.2026.10247 Published online by Cambridge University Press

to lithostratigraphic boundaries. Ultimately, the validity of this assemblage zone needs to be further tested within a high-resolution sequence-stratigraphic framework, which is currently unavailable.

The HmNj assemblage zone is consistently observed below the AHC assemblage zone, thus providing an additional maximum constraint on the Ediacaran–Cambrian boundary (Fig. 7), which must be above the youngest occurrence of HmNj taxa. The uniserial modular microfossils *H. minor* and *N. jiumenensis* are known to have their last occurrences limited to strata that are independently constrained to be latest Ediacaran in age (e.g., Dong et al., 2008; Luo and Miao, 2020; Chai et al., 2021; Yi et al., 2022), disappearing prior to the Cambrian. We note that Chen and Feng (2019) reported occurrences of *H. minor* from purported Cambrian strata in the Liuchapo Formation at the slope section of Sifangjing; however, no AHC acritarchs have been described from this section, and it remains possible that the HmNj-bearing strata at Sifangjing is terminal Ediacaran in age. In all other South China sections studied thus far, HmNj fossils are restricted to the terminal Ediacaran of the Liuchapo Formation (e.g., Dong et al., 2009; Yi et al., 2022; Chen et al., 2023; Zhang et al., 2023; Luo and Zhu, 2025; this study).

In successions where HmNj and AHC taxa both occur, they may be used to bracket the Ediacaran–Cambrian boundary to a meter-scale resolution in some cases (Fig. 7). However, this precise biostratigraphic definition of the boundary may only be applied in the silicified stratigraphy of the shelf margin and basin of the Yangtze Craton due to the facies dependence of HmNj taxa, which are not preserved in the carbonate-dominated shelf facies. Given the recovered relationship between the HmNj and AHC taxa in sections where they occur together, the last occurrence of *N. jiumenensis* may be used as a proxy for the terminal Ediacaran (Chen et al., 2023). Because the last occurrence of HmNj assemblage taxa may precede the first occurrence of AHC taxa by a notable volume of strata (Fig. 7), the disappearance of HmNj taxa alone is not utilized as a direct boundary proxy.

This study establishes the first occurrence of early Cambrian acanthomorphic acritarchs, alongside the disappearance of Ediacaran modular taxa, as an accurate estimation for the Ediacaran–Cambrian boundary across the Yangtze Craton in South China. Early Cambrian acritarchs demonstrate a wide facies distribution across carbonate and fine-grained siliciclastic successions, a short stratigraphic range, and can be correlated with alternative boundary definitions, including SSF assemblage zones and geochemical proxies (Fig. 7). AHC taxa are more frequently preserved across the Yangtze Craton than either SSFs or the BACE (Jiang et al., 2012; Ahn and Zhu, 2017). Consequently, it is proposed here that the first occurrence of AHC assemblage zone taxa can be adopted as a subsidiary, or even major, marker of the Ediacaran–Cambrian boundary in South China.

Whether the biostratigraphic significance of terminal Ediacaran and earliest Cambrian microfossil taxa, as evidenced in South China, is globally applicable remains to be established. AHC-type taxa are recognized worldwide and have previously been utilized to establish biostratigraphic regimes (Moczydłowska, 1991). *Nenoxites*, in addition to other late Ediacaran modular fossils such as *Palaeopascichnus* Palij, 1976, and *Shaanxilithes* Xing et al., 1984, also demonstrate global distributions (e.g., Psarras et al., 2023; Pinto et al., 2025) and have previously been proposed as potential index fossils for latest Ediacaran successions (e.g., Meyer et al., 2012; Chai et al., 2021). Despite recognition of the potential of these fossils for use in biostratigraphy, adequate assessment of their global application has not been undertaken. The effectiveness of acanthomorphic acritarch biostratigraphy and, to a lesser extent, associated modular fossils, in constraining the Ediacaran–Cambrian boundary across the Yangtze Craton in South China prompts further investigations into globally representative successions to establish the feasibility of applying this biostratigraphic proxy worldwide.

## Conclusions

Recent discoveries have raised considerable questions surrounding the reliability of using the trace fossil *Treptichnus pedum* to define the base of the Cambrian. In certain Ediacaran–Cambrian deposits, such as those in South China, *T. pedum* is an unreliable and unsuitable marker of the boundary. Investigations of stratigraphic successions across the Yangtze Craton of South China have revealed a supplemental biostratigraphic definition. Early Cambrian acanthomorphic acritarchs characteristic of the AHC assemblage (i.e., *Asteridium tornatum*, *Heliosphaeridium ampliatum*, and *Comasphaeridium annulare*) are recovered from 11 of 14 analyzed Yangtze Craton sections, representing a diverse range of lithologies and depositional environments. Acritarch occurrences are shown to correlate with the first SSF assemblage zone in South China as well as the globally recognized BACE, both representing alternatives to *T. pedum* for recognizing the Ediacaran–Cambrian boundary. Thus, the first occurrence of AHC taxa is demonstrated to approximate the Ediacaran–Cambrian boundary. Additional identification of the Ediacaran modular microfossils *Horodyskia minor* and *Nenoxites jiumenensis* (collectively the HmNj assemblage zone) in the stratigraphy underlying the AHC assemblage zone allows the boundary to be bracketed to a meter-scale resolution. The regionally consistent stratigraphic pattern of the AHC and HmNj assemblage biozones is demonstrated here to provide reliable biostratigraphic constraints on the Ediacaran–Cambrian boundary in South China, calling for a global test of these biostratigraphic markers.

## Systematic paleontology

The systematic paleontology of small shelly fossils follows the International Code of Zoological Nomenclature (ICZN: https://www.iczn.org/the-code/the-code-online/; accessed February 1, 2026); for all other fossils, we follow the International Code of Nomenclature for Algae, Fungi, and Plants (ICNAFP: https://www.iaptglobal.org/_functions/code/madrid; accessed February 1, 2026). Additional systematics may be found in the supplementary materials.

## Acritarchs

Group **Acritarcha** Evitt, 1963

Genus ***Heziaosphaera*** new genus

*Type species.* *Heziaosphaera bimorphospina* n. gen. n. sp.

*Diagnosis.* Same as species.

*Etymology.* From the discovery locality at Hezi'ao and the Greek sphaîra, regarding the spheroidal vesicles.

*Remarks.* *Heziaosphaera* n. gen. is erected to accommodate small acanthomorphic acritarchs exhibiting bimorphic processes, or processes of two distinct morphologies. Large bimorphic acritarchs are known from Ediacaran deposits (Shang and Liu, 2024); however,

https://doi.org/10.1017/jpa.2026.10247 Published online by Cambridge University Press

early Paleozoic bimorphic or heteromorphic acritarchs are rare (e.g., Jain, 2020; Shan et al., 2022). Small, morphologically complex, Phanerozoic acritarchs that exhibit bimorphic processes do not generally appear until the latest Cambrian (Downie, 1982) or Ordovician–Silurian (e.g., Eisenack et al., 1973; Mendelson, 1987). This is the first early Cambrian acritarch to exhibit bimorphic processes from South China.

***Heziaosphaera bimorphospina*** new species
Figure 8.3, 8.4

*Type.* The specimen illustrated in Figure 8.3 is designated as the holotype, reposited at Virginia Polytechnic Institute Geosciences Museum, with a museum catalog number of VPIGM–4849.

*Material.* Eleven specimens identified from the Yanjiahe Formation at Hezi'ao, South China.

*Diagnosis.* Small acritarchs exhibiting bimorphic processes. Small processes are short, numerous, densely distributed, radially arranged, and apparently solid. Large processes are long, evenly but sparsely distributed, stiff, hollow, and conical.

*Description.* Spherical to ovate vesicles measuring 7.9–11.7 μm in diameter (mean = 9.0 μm, s.d. = 1.1 μm, n = 11). Large, conical processes are 8.1–17.5 μm (mean = 11.3 μm, s.d. = 2.7 μm) in length and 0.8–2.3 μm (mean = 1.4 μm, s.d. = 0.4 μm) in basal width. They are evenly distributed on complete specimens, separated by ~2–6 μm. Number of observed longer processes varies between 4 and 7, with an average of 5 per specimen. Shorter processes are 0.8–2.7 μm (mean = 1.5 μm, s.d. = 0.5 μm) in length and <0.2 μm in width; they are evenly but densely distributed, separated by <0.5 μm.

*Etymology.* From the Latin bi, meaning two; the Greek morph, meaning form or shape; and the Latin spina, referring to the two distinct process morphologies.

*Remarks. Heziaosphaera bimorphospina* n. gen. n. sp. exhibits process morphologies similar to those of co-occurring *H. ampliatum* and *C. annulare*. The larger processes of *H. bimorphospina* are reminiscent of the spines exhibited by *Heliosphaeridium ampliatum*, although they are less numerous and comparably longer than those of *H. ampliatum*. The smaller, hair-like processes of *H. bimorphospina* can be compared to those of *C. annulare*, but those of the latter are generally slightly longer.

Microfossils similar to those described here may have previously been identified in early Cambrian strata of South China (Wang, 1985, fig. 3:6, 3:10, 3:11). However, these microfossils were defined as possessing short, dense, and radially arranged processes; no mention of larger, straight spines was made in their original description. Due to the poor image quality and the uncertainty in identifying the larger processes, it is unclear whether these specimens belong to *H. bimorphospina*.

## Incertae Sedis

Genus ***Nenoxites*** Fedonkin, 1976

*Type species. Nenoxites curvus* Fedonkin, 1976

*Remarks.* It has previously been argued that Ediacaran fossils from South China assigned to the genus *Palaeopascichnus* exhibit features consistent with a classification within the genus *Nenoxites* (e.g., Luo and Miao, 2020; Yi et al., 2022), but this has not been formalized. The genus *Nenoxites* was originally identified and described as a trace fossil consisting of a series of alternating, curved, transverse grooves and ridges (Fedonkin, 1976). *Palaeopascichnus* exhibits similar morphological features (Palij, 1976), but these genera can be differentiated by their grooves and ridges (Luo and Miao, 2020). *Nenoxites* was defined based on the observation that the curved elements did not always extend across the lateral width of the fossil but could be shifted laterally or centered (Urbanek and Rozanov, 1983). The chamber-like elements of *Palaeopascichnus* extend to the edge of the fossil and demonstrate rounded edges, rather than points, and the chain of elements can branch dichotomously (Kolesnikov et al., 2018). Thus, because *Palaeopascichnus jiumenensis* Dong et al., 2008, *P. minimus* Shen et al., 2007, and *P. meniscatus* Shen et al., 2007, are observed to have crescent segments with sharp ends, convex sides pointing in the same direction, and a small gap between adjacent segments, reassignment to the genus *Nenoxites* is appropriate (Yi et al., 2022), and three new combinations —*Nenoxites minimus* (Shen et al., 2007) n. comb., *Nenoxites meniscatus* (Shen et al., 2007) n. comb., and *Nenoxites jiumenensis* (Dong et al., 2008) n. comb.—are formalized here.

Examples from South China have also been argued to exhibit morphological features distinct from either *Palaeopascichnus* or *Nenoxites*, such as a circular terminal structure, resulting in the erection of the new genus *Ordinilunulatus* Liu et al., 2022, to accommodate these fossils. However, these distinctive features, including variations in the halo surrounding the segments, the total length of the fossils, the number of segments per chain, the presence of a circular terminal structure, and the presence of a filament, vary between specimens. Thus, such variations may represent taphonomic artifacts or observational variations (e.g., a saucer-shaped segment may appear crescent or circular in thin section, depending on its orientation relative to the thin section), and they are not considered taxonomically informative. Consequently, the genus *Nenoxites* is favored here for the South China fossils.

***Nenoxites jiumenensis*** (Dong et al., 2008) n. comb.
Figure 4.3, 4.4

2008 *Palaeopascichnus jiumenensis* Dong et al., p. 372, fig. 7.
2012 *Palaeopascichnus* cf. *jiumenensis*, Dong et al., p. 605, fig. 4A–D.
2020 *Nenoxites* sp., Luo and Miao, p. 9, fig. 8C–E.
2022 *Nenoxites jishouensis* Yi et al., p. 5, fig. 4A, B, E–I.
2022 *Nenoxites irregularis* Yi et al., p. 5, fig. 4J–M.
2022 *Ordinilunulatus jiumenensis* Liu et al., p. 9, fig. 7A–H.

*Holotype.* Specimen in Dong et al. (2008, fig. 7f); 06JM–3, VPIGM–4611.

*Material.* A total of 464 specimens from the Liuchapo Formation at the Ganziping, Daping, Siduping, Xugongping, Louyixi, Longbizui, Taoying, and Jianxincun sections.

*Occurrence.* Upper Ediacaran in South China, including the Liuchapo Formation in Guizhou and Hunan provinces (Dong et al., 2008; Luo and Miao, 2020; Yi et al., 2022; Liu et al., 2022) and the Piyuancun Formation in southern Anhui Province (Dong et al., 2012).

*Description.* A series of uniserially arranged saucer-shaped segments. Segments are 97.1–444.4 μm in width (mean = 226.0 μm,

https://doi.org/10.1017/jpa.2026.10247 Published online by Cambridge University Press

s.d. = 72.0 μm, *n* = 100) and 20.5–175.3 μm in thickness (mean = 59.0 μm, s.d. = 31.3 μm). The series may include a spherical terminal segment, but this is rarely preserved and may in fact represent the transverse cut through a saucer-shaped segment. The concave side of the discoidal segments is oriented in the same direction, with the spherical terminal segment located at the concave end of the series, if present. There are 4–21 (mean = 6, s.d. = 3.1, n = 41) segments per series, spaced by 12.2–368.3 μm (mean = 79.3 μm, s.d. = 64.7 μm, n = 110). Spacing between segments remains approximately constant within each series. Some segments are shifted laterally away from the central axis of the series. Most series are curved or sinuous. Branching is never observed. Width remains approximately constant throughout the series. Segments may be surrounded by a halo of light-colored microcrystalline quartz and connected by a filament.

*Remarks.* *Palaeopascichnus jiumenensis* was initially described by Dong et al. (2008), characterized by its series of meniscate-shaped structures that are arranged uniserially and may demonstrate a spherical terminating segment. This description can be applied to several reported occurrences of uniserially arranged meniscate-shaped chain structures from South China that have been variously assigned to different genera and species. *Nenoxites* sp. (Luo and Miao, 2020, fig. 3F–G) was differentiated from previously identified *Palaeopascichnus* because Luo and Miao (2020) determined that their specimens exhibited crescent elements with sharpened ends and a sideward shift of individual elements away from the central string axis, in some examples. This description is more consistent with the genus *Nenoxites* than *Palaeopascichnus* (Fedonkin, 1976).

The illustrated fossils of Dong et al. (2008, fig. 7) exhibit the *Nenoxites*-type features identified by Luo and Miao (2020), indicating that they also belong to the genus *Nenoxites*. The taxa *N. jishouensis* and *N. irregularis* erected by Yi et al. (2022) were differentiated according to their preservation in three dimensions, although slight differences in segment morphology and separation of elements were also noted. However, *Nenoxites jiumenensis* specimens demonstrate considerable variability according to the quality of their preservation (e.g., Yi et al., 2022, fig. 4), making it challenging to differentiate morphologically similar taxa into biologically meaningful species according to measurement differences that may be a consequence of taphonomy. *Nenoxites jishouensis* and *N. irregularis* were differentiated from *N. jiumenensis* based on the absence of a spherical terminal element, a feature that is here deemed taxonomically unreliable, as discussed above. Thus, these three species are regarded as synonyms. Similarly, the transfer of *Palaeopascichnus jiumenensis* or *Nenoxites jiumenensis* to *Ordinilunulatus jiumenensis* by Liu et al. (2022) on the basis of the presence of a circular terminal element is also questionable. Thus, we choose to adopt the combination of *Nenoxites jiumenensis*.

**Acknowledgments.** We are grateful to Q. Tang (Nanjing University), K. Pang (Nanjing Institute of Geology and Paleontology), B. Wan (Northwest University), and M. Meyer (Virginia Tech) for assisting with fieldwork. We thank Associate Editor J. Botting, reviewer X. Shang, and an anonymous reviewer for constructive comments. Portions of this manuscript were adapted from K. O'Donnell's Master's thesis (O'Donnell, 2013), titled *Constraining the Ediacaran–Cambrian boundary in South China using acanthomorphic acritarchs and Palaeopascichnus fossils*, defended at Virginia Tech in 2013. This study was supported by the Virginia Tech Department of Geosciences (OMLD, KO'D), Virginia Tech Institute for Critical Technology and Applied Sciences (OMLD), AASP – The Palynological Society (OMLD), the National Science Foundation (EAR-2021207 and DEB-2449385, SX), and the Virginia Polytechnic Institute Geosciences Museum.

**Competing interests.** The authors declare no competing interests.

**Data availability statement.** Supplementary data, including additional systematic paleontology and a fossil occurrences data table, are available at the Dryad Digital Repository: https://datadryad.org/dataset/doi:10.5061/dryad.6wwpzgndp.

## References

**Ahn, S.Y., and Zhu, M.**, 2017, Lowermost Cambrian acritarchs from the Yanjiahe Formation, South China: implication for defining the base of the Cambrian in the Yangtze Platform: *Geological Magazine*, **v. 154**, p. 1217–1231.

**Alroy, J.**, 2010, The shifting balance of diversity among major marine animal groups: *Science*, **v. 329**, p. 1191–1194.

**Babcock, L.E., Peng, S., Zhu, M., Xiao, S., and Ahlberg, P.**, 2014, Proposed reassessment of the Cambrian GSSP: *Journal of African Earth Sciences*, **v. 98**, p. 3–10.

**Broce, J., Schiffbauer, J.D., Sharma, K.S., Wang, G., and Xiao, S.**, 2014, Possible animal embryos from the Lower Cambrian (Stage 3) Shuijingtuo Formation, Hubei Province, *South China:* Journal of Paleontology, **v. 88**, p. 385–394.

**Buatois, L.A.**, 2018, *Treptichnus pedum* and the Ediacaran–Cambrian boundary: significance and caveats: *Geological Magazine*, **v. 155**, p. 174–180.

**Buatois, L.A., Almond, J., and Germs, G.J.B.**, 2013, Environmental tolerance and range offset of *Treptichnus pedum*: implications for the recognition of the Ediacaran–Cambrian boundary: *Geology*, **v. 41**, p. 519–522.

**Chai, S., Wu, Y., and Hua, H.**, 2021, Potential index fossils for the Terminal Stage of the Ediacaran System: *Journal of Asian Earth Sciences*, **v. 218**, 104885, https://doi.org/10.1016/j.jseaes.2021.104885.

**Chang, S., Zhang, L., Clausen, S., Bottjer, D.J., and Feng, Q.**, 2019, The Ediacaran-Cambrian rise of siliceous sponges and development of modern oceanic ecosystems: *Precambrian Research*, v. **333**, 105438.

**Chang, S., Zhang, L., and Feng, Q.**, 2025, Diverse organic-walled microfossils from the basal Cambrian Yanjiahe Formation in the eastern Three Gorges area: *Review of Palaeobotany and Palynology*, **v. 340**, 105361, https://doi.org/10.1016/j.revpalbo.2025.105361.

**Chen, C., and Feng, Q.**, 2019, Carbonate carbon isotope chemostratigraphy and U–Pb zircon geochronology of the Liuchapo Formation in South China: constraints on the Ediacaran–Cambrian boundary in deep-water sequences: *Palaeogeography, Palaeoclimatology, Palaeoecology*, **v. 535**, 109361, https://doi.org/10.1016/j.palaeo.2019.109361.

**Chen, C., Feng, Q., Algeo, T.J., Zhang, L., Chang, S., and Li, M.**, 2023, New sponge spicules from the Ediacaran–Cambrian transition in deep-water facies of South China: *Palaeogeography, Palaeoclimatology, Palaeoecology*, **v. 627**, 111714, https://doi.org/10.1016/j.palaeo.2023.111714.

**Chen, D., Wang, J., Qing, H., Yan, D., and Li, R.**, 2009, Hydrothermal venting activities in the early Cambrian, South China: petrological, geochronological and stable isotopic constraints: *Chemical Geology*, **v. 258**, p. 168–181.

**Chen, D., Zhou, X., Fu, Y., Wang, J., and Yan, D.**, 2015, New U–Pb zircon ages of the Ediacaran–Cambrian boundary strata in South China: *Terra Nova*, **v. 27**, p. 62–68.

**Chen, M., Xiao, Z., and Yuan, X.**, 1994, A new assemblage of megafossils – Miaohe biota from Upper Sinian Doushantuo Formation, Yangtze Gorges: *Acta Palaeontologica Sinica*, **v. 33**, p. 391–403.

**Chen P.**, 1984, Discovery of lower Cambrian small shelly fossils from Jijiapo, Yichang, West Hubei and its significance: *Professional Papers of Stratigraphy and Palaeontology*, **v. 13**, p. 49–64.

**Compston, W., Zhang, Z., and Cooper, J.A.**, 2008, Further SHRIMP geochronology on the early Cambrian of South China: *American Journal of Science*, **v. 208**, p. 399–420.

**Condon, D., Zhu, M., Bowring, S., Wang, W., Yang, A., and Jin, Y.**, 2005, U–Pb ages from the Neoproterozoic Doushantuo Formation, China: *Science*, **v. 308**, p. 95–98.

**Ding, L., Li, Y., and Chen, H.**, 1992, Discovery of *Micrhystridium regulare* from Sinian–Cambrian boundary strata in Yichang, Hubei, and its stratigraphic significance: *Acta Micropalaeontologica Sinica*, **v. 9**, p. 303–309.

**Dong, L., Xiao, S., Shen, B., and Zhou, C.**, 2008, Silicified *Horodyskia* and *Palaeopascichnus* from upper Ediacaran cherts in South China: tentative

phylogenetic interpretation and implications for evolutionary stasis: *Journal of the Geological Society of London*, **v. 165**, p. 367–378.

**Dong, L., Xiao, S., Shen, B., Zhou, C., Li, G., and Yao, J.**, 2009, Basal Cambrian microfossils from the Yangtze Gorges area (South China) and the Aksu area (Tarim Block, northwestern China): *Journal of Paleontology*, **v. 83**, p. 30–44.

**Dong, L., Song, W., Xiao, S., Yuan, X., Chen, Z., and Zhou, C.**, 2012, Micro- and macrofossils from the Piyuancun Formation and their implications for the Ediacaran–Cambrian boundary in southern Anhui: *Journal of Stratigraphy*, **v. 36**, p. 600–610.

**Downie, C.**, 1982, Lower Cambrian acritarchs from Scotland, Norway, Greenland and Canada: *Transactions of the Royal Society of Edinburgh: Earth Sciences*, **v. 72**, p. 257–295.

**Eisenack, A., Cramer, F.H., Díez, M.d.C.R.**, 1973, *Katalog der Fossilen Dinoflagellaten, Hystrichosphären und Verwandten Mikrofossilien, Band III, Acritarcha 1. Teil. E*: Stuttgart, Schweizerbart'sche Verlagsbuchhandlung.

**Evitt, W.R.**, 1963, A discussion and proposals concerning fossil dinoflagellates, hystrichospheres, and acritarchs: *Proceedings of the National Academy of Sciences, USA*, **v. 49**, p. 158–164; 298–302.

**Fedonkin, M.A.**, 1976, Trace fossils of metazoans from Valdai Group: *Izvestiya Akademii Nauk SSSR, Seriya Geologicheskaya*, **v. 4**, p. 129–132.

**Gehling, J.G., Jensen, S., Droser, M.L., Myrow, P.M., and Narbonne, G.M.**, 2001, Burrowing below the basal Cambrian GSSP, Fortune Head, Newfoundland: *Geological Magazine*, **v. 138**, p. 213–218.

**Geyer, G.**, 2005, The Fish River Subgroup in Namibia: stratigraphy, depositional environments and the Proterozoic–Cambrian boundary problem revisited: *Geological Magazine*, **v. 142**, p. 465–498.

**Geyer, G., and Uchman, A.**, 1995, Ichnofossil assemblages from the Nama Group (Neoproterozoic–Lower Cambrian) in Namibia and the Proterozoic–Cambrian boundary problem revisited, *in* Geyer, G., and Landing, E., eds., Morocco '95: The Lower–Middle Cambrian Standard of Western Gondwana: *Beringeria Special Issue*, **v. 2**, p. 175–202.

**Gnilovskaya, M.B.**, 1971, Drevnejshie vodnye rasteniya venda Russkojplatformy [The oldest Vendian aquatic plants on the Russian platform]: *Palaeontologicheskij Zhurnal*, **v. 3**, p. 101–107.

**Grabau, A.W.**, 1900., Palaeontology of the Cambrian terranes of the Boston Basin: *Occasional Papers of the Boston Society of Natural History*, **v. 4**, p. 601–694.

**Guo, J., Li, Y., Han, J., Zhang, X., Zhang, Z., Ou, Q., Liu, J., Shu, D., Maruyama, S., and Komiya, T.**, 2008, Fossil association from the lower Cambrian Yanjiahe Formation in the Yangtze Gorges area, Hubei, South China: *Acta Geologica Sinica (Chinese Edition)*, **v. 82**, p. 1124–1132.

**Guo, J., Li, Y., Han, H., Ou, Q., Zhou, J., and Zheng, Y.**, 2012, New macroscopic problematic fossil from the early Cambrian Yanjiahe biota, Yichang, Hubei, China: *Acta Geologica Sinica–English Edition*, **v. 86**, p. 791–798.

**Guo, J., Li, Y., and Li, G.**, 2014, Small shelly fossils from the early Cambrian Yanjiahe Formation, Yichang, Hubei, China: *Gondwana Research*, **v. 25**, p. 999–1007.

**Guo, J.-F., Li, G.-X., Qiang, Y.-Q., Song, Z.-C., Zhang, Z.-F., Han, J., and Wang, W.-Z.**, 2021, *Watsonella crosbyi* from the lower Cambrian (Terreneuvian, Stage 2) Yanjiahe Formation in Three Gorges area, South China: *Palaeoworld*, **v. 30**, p. 1–19.

**Guo, Q., Strauss, H., Zhu, M., Zhang, J., Yang, X., Lu, M., and Zhao, F.**, 2013, High resolution organic carbon isotope stratigraphy from a slope to basinal setting on the Yangtze Platform, South China: implications for the Ediacaran–Cambrian transition: *Precambrian Research*, **v. 225**, p. 209–217.

**Herringshaw, L.G., Callow, R.T., and McIlroy, D.**, 2017, Engineering the Cambrian explosion: the earliest bioturbators as ecosystem engineers: *Geological Society of London Special Publications*, **v. 448**, p. 369–382.

**Huang, T., Chen, D., Ding, Y., Zhou, X. and Zhang, G.**, 2020, SIMS U–Pb zircon geochronological and carbon isotope chemostratigraphic constraints on the Ediacaran–Cambrian boundary succession in the Three Gorges area, South China: *Journal of Earth Science*, **v. 31**, p. 69–78.

**Huntley, J.W., Xiao, S., and Kowalewski, M.**, 2006, 1.3 billion years of acritarch history: an empirical morphospace approach: *Precambrian Research*, **v. 144**, p. 52–68.

**Ishikawa, T., Ueno, Y., Komiya, T., Sawaki, Y., Han, J., Shu, D., Li, Y., Maruyama, S., and Yoshida, N.**, 2008, Carbon isotope chemostratigraphy of a Precambrian/Cambrian boundary section in the Three Gorge area, South China: prominent global-scale isotope excursions just before the Cambrian Explosion: *Gondwana Research*, **v. 14**, p. 193–208.

**Jain, S.**, 2020, Acritarchs, *in* Jain, S., *Fundamentals of Invertebrate Palaeontology*: New Delhi, Springer, p. 27–42.

**Jenkins, R.J.F., Cooper, J.A., and Compston, W.**, 2002, Age and biostratigraphy of early Cambrian tuffs from SE Australia and southern China: *Journal of the Geological Society, London*, **v. 159**, p. 645–658.

**Jensen, S.**, 1997, Trace fossils from the lower Cambrian Mickwitzia Sandstone, south-central Sweden: *Fossils & Strata*, **v. 42**, p. 1–111.

**Jiang, G., Shi, X., Zhang, S., Wang, Y., and Xiao, S.**, 2011, Stratigraphy and paleogeography of the Ediacaran Doushantuo Formation (ca. 635–551 Ma) in South China: *Gondwana Research*, **v. 19**, p. 831–849.

**Jiang, G., Wang, X., Shi, X., Xiao, S., Zhang, S., and Dong, J.**, 2012, The origin of decoupled carbonate and organic carbon isotope signatures in the early Cambrian (ca. 542–520 Ma) Yangtze Platform: *Earth and Planetary Science Letters*, **v. 317**, p. 96–110.

**Jiang, S.-Y., Pi, D.-H., Heubeck, C., Frimmel, H., Liu, Y.-P., Deng, H.-L., Ling, H.-F., and Yang, J.-H.**, 2009, Early Cambrian ocean anoxia in South China: *Nature*, **v. 459**, E5–E6, https://doi.org/10.1038/nature08048.

**Kirjanov, V.V.**, 1974, Novye akritarhki iz kembrijshikh otlozhenij Volyni [New acritarchs from the Cambrian deposits of Volhynia]: *Paleontologicheskij Zhurnal*, **v. 2**, p. 117–130.

**Knoll, A.H.**, 1994, Proterozoic and early Cambrian protists: evidence for accelerating evolutionary tempo: *Proceedings of the National Academy of Sciences, USA*, **v. 91**, p. 6743–6750.

**Kolesnikov, A.V., Rogov, V.I., Bykova, N.V., Danelian, T., Clausen, S., Maslov, A.V., and Grazhdankin, D.V.**, 2018, The oldest skeletal macroscopic organism *Palaeopascichnus linearis*: *Precambrian Research*, **v. 316**, p. 24–37.

**Landing, E.**, 1994, Precambrian–Cambrian boundary global stratotype ratified and a new perspective of Cambrian time: *Geology*, **v. 22**, p. 179–182.

**Landing, E., Geyer, G., Brasier, M.D., and Bowring, S.A.**, 2013, Cambrian evolutionary radiation: context, correlation, and chronostratigraphy: overcoming deficiencies of the first appearance datum (FAD) concept: *Earth-Science Reviews*, **v. 123**, p. 133–172.

**Li, G., and Holmer, L.E.**, 2004, Early Cambrian lingulate brachiopods from the Shaanxi Province, China: *GFF*, **v. 126**, p. 193–211.

**Li, G., Zhu, M., Steiner, M., and Qian, Y.**, 2004, Skeletal faunas from the Qiongzhusian of southern Shaanxi: biodiversity and lithofacies–biofacies links in the lower Cambrian carbonate settings: *Progress in Natural Science*, **v. 14**, 91–96, https://doi.org/10.1080/10020070412331343201.

**Li, G., Steiner, M., Zhu, M., and Zhao, X.**, 2012, Early Cambrian eodiscoid trilobite *Hupeidiscus orientalis* from South China: ontogeny and implications for affinities of *Mongolitubulus*-like sclerites: *Bulletin of Geosciences*, **v. 87**, 159–169, https://doi.org/10.3140/bull.geosci.1224.

**Ling, H.F., Feng, H.Z., Pan, J.Y., Jiang, S.Y., Chen, Y.Q., and Chen, X.**, 2007, Carbon isotope variation through the Neoproterozoic Doushantuo and Dengying formations, South China: implications for chemostratigraphy and paleoenvironmental change: *Palaeogeography, Palaeoclimatology, Palaeoecology*, **v. 254**, p. 158–174.

**Linnemann, U., Ovtcharova, M., Schaltegger, U., Gärtner, A., Hautmann, M.**, et al., 2019, New high-resolution age data from the Ediacaran–Cambrian boundary indicate rapid, ecologically driven onset of the Cambrian explosion: *Terra Nova*, **v. 31**, p. 49–58.

**Liu, H., Dong, L., Qin, S.J., Liu, W., and Li, C.Q.**, 2022, Restudy of string fossils from the Ediacaran–Cambrian Liuchapo Formation in Guizhou Province, South China: *Precambrian Research*, **v. 376**, 106693, https://doi.org/10.1016/j.precamres.2022.106693.

**Liu, J., Jiang, Q., Zhang, Y., Liu, J., Ai, Y., Duan, P., and Zhu, G.**, 2025, Earliest Cambrian carbonate platform evolution, environmental change, and organic matter accumulation in the northwestern Yangtze Block, South China: *Minerals*, **v. 15**, 812, https://doi.org/10.3390/min15080812.

**Luo, C., and Miao, L.Y.**, 2020, A *Horodyskia-Nenoxites*-dominated fossil assemblage from the Ediacaran–Cambrian transition (Liuchapo Formation, Hunan Province): its paleontological implications and stratigraphic potential: *Palaeogeography Palaeoclimatology Palaeoecology*, **v. 545**, 109635, https://doi.org/10.1016/j.palaeo.2020.109635.

**Luo, C., and Reitner, J.**, 2019, Three-dimensionally preserved stem-group hexactinellid sponge fossils from lower Cambrian (Stage 2) phosphorites of China: *PalZ*, **v. 93**, p. 187–194.

https://doi.org/10.1017/jpa.2026.10247 Published online by Cambridge University Press

**Luo, C., and Zhu, M.**, 2025, Chert Lagerstätten as a new window to the biological revolution across the Ediacaran–Cambrian boundary: *Geology*, **v. 53**, p. 467–472.

**Luo, H., Jiang, Z., Wu, X., Song, X., and Ouyang, L.**, 1982, *The Sinian–Cambrian Boundary in Eastern Yunnan, China*: Kunming, People's Publishing House of Yunnan, 265 p.

**Luo, M., Brock, G.A., Liang, Y., Song, B., Hu, Y., Liu, F., and Zhang, Z.**, 2024, Correlation and stratigraphic implications of the lowermost Cambrian small shelly fossils from new sites of South China: *Journal of the Geological Society*, **v. 181**, p. 2023–2231.

**Maloof, A.C., Porter, S.M., Moore, J.L., Dudás, F.Ö., Bowring, S.A., Higgins, J.A., Fike, D.A., and Eddy, M.P.**, 2010, The earliest Cambrian record of animals and ocean geochemical change: *Geological Society of America Bulletin*, **v. 122**, p. 1731–1774.

**Mángano, M.G., and Buatois, L.A.**, 2017, The Cambrian revolutions: trace-fossil record, timing, links and geobiological impact: *Earth-Science Reviews*, **v. 173**, p. 96–108.

**Mendelson, C.V.**, 1987, Acritarchs: *Notes for a Short Course: Fossil Prokaryotes and Protists: Studies in Geology*, **v. 18**, p. 62–86.

**Meyer, M., Schiffbauer, J.D., Xiao, S., Cai, Y., and Hua, H.**, 2012, Taphonomy of the upper Ediacaran enigmatic ribbonlike fossil *Shaanxilithes*: *Palaios*, **v. 27**, p. 354–372.

**Moczydłowska, M.**, 1988, New lower Cambrian acritarchs from Poland: *Review of Palaeobotany and Palynology*, **v. 54**, p. 1–10.

**Moczydłowska, M.**, 1991, Acritarch biostratigraphy of the lower Cambrian and the Precambrian–Cambrian boundary in southeastern Poland: *Fossils and Strata*, **v. 29**, p. 1–127.

**Moczydłowska, M.**, 2011, The early Cambrian phytoplankton radiation: acritarch evidence from the Lükati Formation, Estonia: *Palynology*, **v. 35**, p. 103–145.

**Moczydłowska, M., and Zang, W.-L.**, 2006, The early Cambrian acritarch *Skiagia* and its significance for global correlation: *Palaeoworld*, **v. 15**, p. 328–347.

**Narbonne, G.M., Myrow, P.M., Landing, E., and Anderson, M.M.**, 1987, A candidate stratotype for the Precambrian–Cambrian boundary, Fortune Head, Burin Peninsula, southeastern Newfoundland: *Canadian Journal of Earth Sciences*, **v. 24**, p. 1277–1293.

**Nowak, H., Servais, T., Monnet, C., Molyneux, S.G., and Vandenbroucke, T. R.A.**, 2015, Phytoplankton dynamics from the Cambrian Explosion to the onset of the Great Ordovician Biodiversification Event: a review of Cambrian acritarch diversity: *Earth-Science Reviews*, **v. 151**, p. 117–131.

**O'Donnell, K.**, 2013, Constraining the Ediacaran–Cambrian boundary in South China using acanthomorphic acritarchs and *Palaeopascichnus* fossils [Master's thesis]: Blacksburg, Virginia Tech, 56 p.

**Palacios, T., and Vidal, G.**, 1992, Lower Cambrian acritarchs from northern Spain: the Precambrian–Cambrian boundary and biostratigraphic implications: *Geological Magazine*, **v. 129**, p. 421–436.

**Palacios, T., Jensen, S., Barr, S.M., White, C.E., and Miller, R.F.**, 2011, New biostratigraphical constraints on the lower Cambrian Ratcliffe Brook Formation, southern New Brunswick, Canada, from organic-walled microfossils: *Stratigraphy*, **v. 8**, p. 45–60.

**Palij, V.M.**, 1976, Remains of non-skeletal fauna and trace fossils from upper Precambrian and lower Cambrian deposits of Podolia, *in* Ryabenko, V.A., ed., *Paleontology and Stratigraphy of the Upper Precambrian and Lower Paleozoic of the South-Western Part of the East European Platform*: Kyiv, Naukova Dumka, p. 63–77

**Peng, S., and Babcock, L.E.**, 2001, Cambrian of the Hunan–Guizhou region, South China, *in* Peng, S., Babcock, L.E., and Zhu, M., eds., *Cambrian System of South China*: Hefei, University of Science and Technology of China Press. *Palaeoworld*, **v. 13**, p. 3–51.

**Peng, S., Babcock, L.E., and Cooper, R.A.**, 2012, The Cambrian Period, *in* Gradstein, F.M., Ogg, J.G., Schmitz, M.D., and Ogg, G.M., eds., *Geological Time Scale 2012*: Oxford, Elsevier, p. 437–488.

**Peng, S., Babcock, L.E., and Ahlberg, P.**, 2020, The Cambrian Period, *in* Gradstein, F.M., Ogg, J.G., Schmitz, M.D., and Ogg, G.M., eds., *Geologic Time Scale 2020*: Oxford, Elsevier, p. 565–629.

**Pinto, A.J., Álvarez-Lloret, P., Callegari, I., and Scharf, A.**, 2025, An Ediacaran trace-like body fossil of a Palaeopascichnus specimen from Oman under 3D micro-tomography: *Facies*, **v. 71**, 13, https://doi.org/10.1007/s10347-025-00705-5.

**Psarras, C., Donoghue, P.C., Garwood, R.J., Grazhdankin, D.V., Parry, L.A., Rogov, V.I., and Liu, A.G.**, 2023, Three-dimensional reconstruction, taphonomic and petrological data suggest that the oldest record of bioturbation is a body fossil coquina: *Papers in Palaeontology*, **v. 9**, e1531, https://doi.org/10.1002/spp2.1531.

**Qian, Y., and Yin, G.**, 1984, Small shelly fossils from the lowest Cambrian in Guizhou: *Professional Papers of Stratigraphy and Palaeontology*, **v. 13**, p. 91–124.

**Seilacher, A.**, 1955, Beiträge zur Kenntnis des Kambriums in der Salt Range (Pakistan). V. Spuren und Fazies im Unterkambrium: *Abhandlungen der mathematisch-naturwissenschaftlichen Klasse der Akademie der Wissenschaften und der Literatur in Mainz*, **v. 1955**, p. 372–399.

**Sergeev, V.N., and Ogurtsova, R.N.**, 1989, Microbiota of the lower Cambrian phosphorite-bearing sediments of Malyi-Karatau (Southern Kazakhstan): *Izvestiya Akademii Nauk SSSR Seriya Geologicheskaya*, **v. 3**, p. 58–66.

**Shan, L., Yan, K., Zhang, Y., Li, J., and Servais, T.**, 2022, Palaeoecology of Cambrian–Ordovician acritarchs from China: evidence for a progressive invasion of the marine habitats: *Philosophical Transactions of the Royal Society B*, **v. 377**, 20210035, https://doi.org/10.1098/rstb.2021.0035.

**Shang, X., and Liu, P.**, 2024, Taxonomic reviews for genera *Megasphaera*, *Membranospinosphaera* and *Spinomargosphaera* of the Ediacaran spheroidal acritarchs: *Precambrian Research*, **v. 407**, 107409, https://doi.org/10.1016/j.precamres.2024.107409.

**Shang, X., Liu, P., Yang, B., and Chen, S.**, 2016, Ecology and phylogenetic affinity of the early Cambrian tubular microfossil *Megathrix longus*: *Palaeontology*, **v. 59**, p. 13–28.

**Shang, X., Liu, P., Moczydłowska, M., and Yang, B.**, 2020, Algal affinity and possible life cycle of the early Cambrian acritarch *Yurtusia uniformis* from South China: *Palaeontology*, **v. 63**, p. 903–917.

**Shen, B., Xiao, S., Dong, L., Zhou, C., and Liu, J.**, 2007, Problematic macrofossils from Ediacaran successions in the North China and Chaidam blocks: implications for their evolutionary roots and biostratigraphic significance: *Journal of Paleontology*, **v. 81**, p. 1396–1411.

**Steiner, M.**, 1996, *Chuaria circularis* Walcott (1899) – "megasphaeromorph acritarch" or prokaryotic colony?: *Acta Universitatis Carolinae Geologica*, **v. 40**, p. 645–665.

**Steiner, M., Mehl, D., Reitner, J., and Erdtmann, B.D.**, 1993, Oldest entirely preserved sponges and other fossils from the lowermost Cambrian and a new facies reconstruction of the Yangtze Platform (China): *Berliner geowissenschaftliche Abhandlungen*, **v. 9**, p. 293–329.

**Steiner, M., Wallis, E., Erdtmann, B.-D., Zhao, Y., and Yang, R.**, 2001, Submarine-hydrothermal exhalative ore layers in black shales from South China and associated fossils – insights into a lower Cambrian facies and bio-evolution: *Palaeogeography, Palaeoclimatology, Palaeoecology*, **v. 169**, p. 165–191.

**Steiner, M., Li, G., Qian, Y., and Zhu, M.**, 2004, Lower Cambrian small shelly fossils of northern Sichuan and southern Shaanxi (China), and their biostratigraphic importance: *Geobios*, **v. 37**, p. 259–275.

**Steiner, M., Li, G., Qian, Y., Zhu, M., and Erdtmann, B.D.**, 2007, Neoproterozoic to early Cambrian small shelly fossil assemblages and a revised biostratigraphic correlation of the Yangtze Platform (China): *Palaeogeography, Palaeoclimatology, Palaeoecology*, **v. 254**, p. 67–99.

**Steiner, M., Yang, B., Hohl, S., Zhang, L., and Chang, S.**, 2020, Cambrian small skeletal fossil and carbon isotope records of the southern Huangling Anticline, Hubei (China) and implications for chemostratigraphy of the Yangtze Platform: *Palaeogeography, Palaeoclimatology, Palaeoecology*, **v. 554**, 10987, https://doi.org/10.1016/j.palaeo.2020.109817.

**Tiwari, M.**, 1999, Organic-walled microfossils from the Chert-phosphorite Member, Tal Formation, Precambrian–Cambrian boundary, India: *Precambrian Research*, **v. 97**, p. 99–113.

**Topper, T.P., Guo, J., Clausen, S., Skovsted, C.B., and Zhang, Z.**, 2019, A stem group echinoderm from the basal Cambrian of China and the origins of Ambulacraria: *Nature Communications*, **v. 10**, 1366, https://doi.org/10.1038/s41467-019-09059-3.

**Topper, T., Betts, M.J., Dorjnamjaa, D., Li, G., Li, L., Altanshagai, G., Enkhbaatar, B., and Skovsted, C.B.**, 2022, Locating the BACE of the Cambrian: Bayan Gol in southwestern Mongolia and global correlation of the Ediacaran–Cambrian boundary: *Earth-Science Reviews*, **v. 229**, 104017, https://doi.org/10.1016/j.earscirev.2022.104017.

https://doi.org/10.1017/jpa.2026.10247 Published online by Cambridge University Press

**Urbanek, A., and Rozanov, A.Y.**, eds., 1983, *Upper Precambrian and Cambrian Palaeontology of the East-European Platform: Contribution of the Soviet–Polish Working Group on the Precambrian–Cambrian Boundary Problem*: Warsaw, Wydawnictwa Geologiczne.

**Vannier, J., Calandra, I., Gaillard, C., and Żylińska, A.**, 2010, Priapulid worms: pioneer horizontal burrowers at the Precambrian–Cambrian boundary: *Geology*, **v. 38**, p. 711–714.

**Volkova, N.A.**, 1968, Akritarkhi dokembrijskikh i nizhnekembrijskikh otlozhenij Estonii [Acritarchs from the Precambrian and Lower Cambrian deposits of Estonia], *in* Volkova, N.A., Zhuravleva, Z.A., Zabrodin, V.E., and Klinger, B. S., ed., Problematiki Pogranichnykh Sloev Rifeya i Kembriya Russkoj Platformy, Urala i Kazakhstana *[*Problematics of Riphean and Cambrian Strata of the Russian Platform, Urals and Kazakhstan*]*: Moscow, Nauka, p. 8–36.

**Voronova, L.G., and Missarzhevsky, V.V.**, 1969, Finds of algae and worm tubes in the Precambrian–Cambrian boundary beds of the northern part of the Siberian Platform: *Doklady Akademii Nauk SSSR*, **v. 184**, p. 207–210.

**Walcott, C.D.**, 1899, Pre-Cambrian fossiliferous formations: *Bulletin of the Geological Society of America*, **v. 10**, p. 199–244.

**Wang, D., Qiang, Y., Guo, J., Vannier, J., Song, Z., Peng, J., Zhang, B., Sun, J., Yu, Y., Zhang, Y., and Zhang, T.**, 2024, Early evolution of the ecdysozoan body plan: *eLife*, **v. 13**, RP94709, https://doi.org/10.7554/eLife.94709.3.

**Wang, F.**, 1985, Middle–upper Proterozoic and lowest Phanerozoic microfossil assemblage from SW China and contiguous areas: *Precambrian Research*, **v. 29**, p. 33–43.

**Wang, J., Chen, D., Yan, D., Wei, H., and Xiang, L.**, 2012, Evolution from an anoxic to oxic deep ocean during the Ediacaran–Cambrian transition and implications for bioradiation: *Chemical Geology*, v. 306–307, p. 129–138.

**Wang, W., Zhou, M., Chu, Z., Xu, J., Li, C., Luo, T., and Guo, J.**, 2020, Constraints on the Ediacaran–Cambrian boundary in deep-water realm in South China: evidence from zircon CA-ID-TIMS U–Pb ages from the topmost Liuchapo Formation: *Science China Earth Sciences*, **v. 63**, p. 1176–1187.

**Wang, X., Shi, X., Jiang, G., and Zhang, W.**, 2012, New U–Pb age from the basal Niutitang Formation in South China: implications for diachronous development and condensation of stratigraphic units across the Yangtze Platform at the Ediacaran–Cambrian transition: *Journal of Asian Earth Sciences*, **v. 48**, p. 1–8.

**Wilson, J.P., Grotzinger, J.P., Fischer, W.W., Hand, K.P., Jensen, S.**, et al., 2012, Deep-water incised valley deposits at the Proterozoic–Cambrian boundary in southern Namibia contain abundant *Treptichnus pedum*: *Palaios*, **v. 27**, p. 252–273.

**Wood, R., and Zhuravlev, A.Y.**, 2012, Escalation and ecological selectivity of mineralogy in the Cambrian Radiation of skeletons: *Earth-Science Reviews*, **v. 115**, p. 249–261.

**Xiang, L., Zhu, Z., Li, S., and Zhou, Z.**, 1999, *Stratigraphy of China: The Cambrian System*: Beijing, Geological Publishing House, 95 p.

**Xing, Y., Ding, Q., Luo, H., He, T., and Wang, Y.**, 1984, The Sinian–Cambrian boundary of China. *Bulletin of the Institute of Geology, Chinese Academy of Geological Sciences*, **v. 10**, p. 1–262.

**Xu, L., Lehmann, B., Mao, J., Qu, W., and Du, A.**, 2011, Re–Os age of polymetallic Ni-Mo-PGE-Au mineralization in early Cambrian black shales of South China—a reassessment: *Economic Geology*, **v. 106**, p. 511–522.

**Yang, B., Steiner, M., Zhu, M., Li, G., Liu, J., and Liu, P.**, 2016, Transitional Ediacaran–Cambrian small skeletal fossil assemblages from South China and Kazakhstan: implications for chronostratigraphy and metazoan evolution: *Precambrian Research*, **v. 285**, p. 202–215.

**Yang, C., Zhu, M., Condon, D.J., and Li, X.-H.**, 2017, Geochronological constraints on stratigraphic correlation and oceanic oxygenation in Ediacaran–Cambrian transition in South China: *Journal of Asian Earth Sciences*, **v. 140**, p. 75–81.

**Yang, C., Bowyer, F.T., Condon, D.J., Li, X.-H., and Zhu, M.Y.**, 2023, New U–Pb age from the Shuijingtuo Formation (Yangtze Gorges area) and its implications for the Cambrian timescale: *Palaeogeography, Palaeoclimatology, Palaeoecology*, **v. 616**, 111477, https://doi.org/10.1016/j.palaeo.2023.111477.

**Yao, J., Xiao, S., Yin, L., Li, G., and Yuan, X.**, 2005, Basal Cambrian microfossils from the Yurtus and Xishanblaq formations (Tarim, north-west China): systematic revision and biostratigraphic correlation of *Micrhystridium*-like acritarchs from China: *Palaeontology*, **v. 48**, p. 687–708.

**Yi, Y.H., Chen, F.Y., Algeo, T.J., and Feng, Q.L.**, 2022, Deep-water fossil assemblages from the Ediacaran–Cambrian transition of western Hunan, South China and their biostratigraphic and evolutionary implications: *Palaeogeography, Palaeoclimatology, Palaeoecology*, **v. 591**, 110878, https://doi.org/10.1016/j.palaeo.2022.110878.

**Yin, L.**, 1987a, Microbiotas of latest Precambrian sequences in China, *in* Nanjing Institute of Geology and Palaeontology, Academia Sinica, *Stratigraphy and Palaeontology of Systemic Boundaries in China, Precambrian-Cambrian Boundary*, Nanjing, Nanjing University Publishing House, **v. 1**, p. 415–494.

**Yin, L.**, 1987b, New data of microfossils from Precambrian–Cambrian cherts in Ningqiang, southern Shaanxi: *Acta Palaeontologica Sinica*, **v. 26**, p. 187–195.

**Yin, L.M., Borjigin, T., Knoll, A.H., Bian, L.Z., Xie, X. M., Bao, F., and Ou, Z. J.**, 2017, Sheet-like microfossils from hydrothermally influenced basinal cherts of the lower Cambrian (Terreneuvian) Niutitang Formation, Guizhou, South China: *Palaeoworld*, **v. 26**, p. 1–11.

**Zamora, S., Wright, D.F., Mooi, R., Lefebvre, B., Guensburg, T.E.**, et al., 2020, Re-evaluating the phylogenetic position of the enigmatic early Cambrian deuterostome *Yanjiahella*: *Nature Communications*, **v. 11**, 1286, https://doi.org/10.1038/s41467-020-14920-x.

**Zang, W.**, 1992, Sinian and early Cambrian floras and biostratigraphy on the South China Platform: *Palaeontographica Abteilung B*, **v. 224**, p. 75–119.

**Zhang, L., Chang, S., Chen, C., Wang, X., Feng, Q. L.**, et al., 2022, *Cloudina* aggregates from the uppermost Dengying Formation, Three Gorges area, South China, and stratigraphical implications: *Precambrian Research*, **v. 370**, 106552, https://doi.org/10.1016/j.precamres.2021.106552.

**Zhang, X., Shu, D., Li, Y., and Han, J.**, 2001, New sites of Chengjiang fossils; crucial windows on the Cambrian explosion: *Journal of the Geological Society of London*, **v. 158**, p. 211–218.

**Zhang, X., Liu, W., and Zhao, Y.**, 2008, Cambrian Burgess Shale-type Lagerstätten in South China: distribution and significance: *Gondwana Research*, **v. 14**, p. 255–262.

**Zhang, Y., Chang, S., Feng, Q., and Zheng, S.**, 2023, A diverse microfossil assemblage from the Ediacaran–Cambrian deep-water chert of the Liuchapo Formation in Guizhou Province, South China: *Journal of Earth Science*, **v. 34**, p. 398–408.

**Zhu, M., Zhang, J., Steiner, M., Yang, A., Li, G., and Erdtmann, B.-D.**, 2003, Sinian–Cambrian stratigraphic framework for shallow- to deep-water environments of the Yangtze Platform: an integrated approach: *Progress in Natural Science*, **v. 13**, p. 951–960.

**Zhu, M., and Li, X.-H.**, 2017, Introduction: from snowball Earth to the Cambrian explosion—evidence from China: *Geological Magazine*, **v. 154**, p. 1187–1192.

**Zhu, M.Y., Yang, A.H., Yuan, J.L., Li, G.X., Zhang, J.M., Zhao, F.C., Ahn, S. Y., and Miao, L.Y.**, 2019, Cambrian integrative stratigraphy and timescale of China: *Science China – Earth Sciences*, **v. 62**, p. 25–60.

**Zhu, R.X., Li, X. H., Hou, X.G., Pan, Y.X., Wang, F., Deng, C.L., and He, H.Y.**, 2009, SIMS U–Pb zircon age of a tuff layer in the Meishucun section, Yunnan, southwest China: constraint on the age of the Precambrian–Cambrian boundary: *Science in China Series D (Earth Science)*, **v. 39**, p. 1105–1111.

https://doi.org/10.1017/jpa.2026.10247 Published online by Cambridge University Press